STRUCTURAL AND ELECTRONIC PROPERTIES OF MONOLAYER AND MULTILAYER GALLIUM NITRIDE CRYSTALS

A THESIS SUBMITTED TO

THE GRADUATE SCHOOL OF ENGINEERING AND SCIENCE

OF BILKENT UNIVERSITY

IN PARTIAL FULFILLMENT OF THE REQUIREMENTS FOR

THE DEGREE OF

MASTER OF SCIENCE

IN

MATERIALS SCIENCE AND NANOTECHNOLOGY

By

Abdullatif Önen

September 2016

Structural and Electronic Properties of Monolayer and Multilayer Gallium Nitride Crystals
By Abdullatif Önen
September 2016

We certify that we have read this thesis and that in our opinion it is fully adequate, in scope and in quality, as a thesis for the degree of Master of Science.

Engin Durgun(Advisor)

Oğuz Gülseren

Hande Toffoli

Approved for the Graduate School of Engineering and Science:

Levent Onural
Director of the Graduate School

ABSTRACT

STRUCTURAL AND ELECTRONIC PROPERTIES OF MONOLAYER AND MULTILAYER GALLIUM NITRIDE CRYSTALS

Abdullatif Önen
M.S. in Materials Science and Nanotechnology
Advisor: Engin Durgun
September 2016

Three-dimensional (3D) Gallium Nitride (GaN) is a III-V compound semiconductor with direct band gap. It is widely used in light emitting diodes (LED) and has potential to be used numerous optoelectronic applications. In this thesis, firstly 3D GaN in wurtzite and zincblende structures are revisited and structural, mechanical, and electronic properties are studied and compared with the literature. Next, the mechanical and electronic properties of two-dimensional (2D) single-layer honeycomb structure of GaN (g-GaN), its bilayer, trilayer and multilayer van der Waals solids are investigated using density functional theory. Based on phonon spectrum analysis and high temperature ab initio molecular dynamics calculations, first it is showed that g-GaN is stable and can preserve its geometry even at high temperatures. Then a comparative study is performed to reveal how the physical properties vary with dimensionality. While 3D GaN is a direct band gap semiconductor, g-GaN in 2D has relatively wider indirect band gap. Moreover, 2D g-GaN displays higher Poisson's ratio and slightly less charge transfer from cation to anion. It is also showed that the physical properties predicted for freestanding g-GaN are preserved when g-GaN is grown on metallic, as well as semiconducting substrates. In particular, 3D layered blue phosphorus being nearly lattice matched to g-GaN is found to be an excellent substrate for growing g-GaN. Bilayer, trilayer and van der Waals crystals can be constructed by special stacking sequence of g-GaN and they can display electronic properties which can be controlled by the number of g-GaN layers. In particular, their fundamental band gap decreases and changes from indirect to direct with increasing number of g-GaN layers. It is hoped that the present work will provide helpful insights for growing g-GaN which can be widely used in nanoelectronics applications in low dimensions.

Keywords: Two-dimensional (2D) materials, gallium nitride (GaN), first principles simulations, density functional theory (DFT).

ÖZET

TEK VE ÇOK ATOMİK KATMAN GALYUM NİTRÜR KRİSTALİNİN YAPISAL VE ELEKTRONİK ÖZELLİKLERİ

Abdullatif Önen
Malzeme Bilimi ve Nanoteknoloji, Yüksek Lisans
Tez Danışmanı: Engin Durgun
Eylül 2016

Üç boyutlu (3B) galyum nitrür direkt band aralıklı bir III-V yarı iletkenidir. Bir çok olası optoelektronik uygulamasının yanında, ışık yayan diyod (LED) olarak da yaygın şekilde kullanılmaktadır. Bu çalışmada ilk olarak 3B wurtzite ve zincblende kristal yapılarındaki GaN'ün yapısal, mekanik, ve elektronik özellikleri gelişen yöntemlerle tekrar hesaplanarak literatürdeki diğer çalışmalarla karşılaştırıldı. Daha sonra, balpeteği örgüsüne sahip iki boyutlu (2B) tek atomik katmanlı GaN'ün (g-GaN) elektronik ve mekanik özellikleri yoğunluk fonksiyonel teori (YFT) kullanılarak incelendi. Buna ek olarak, yine YFT kullanılarak iki atomik katmanlı, üç atomik katmanlı, ve çok atomik katmanlı van der Waals yapıları incelendi. Fonon analizi ve yüksek sıcaklıkta ilk prensipler moleküler dinamik hesaplarıyla yapının kararlı oldugu ve yüksek sıcaklıklarda yapısını koruduğu gösterildi. Devamında fiziksel özelliklerin boyuta bağli olarak değişimi incelendi. 3B GaN direkt bant aralıklı bir yarı iletken olmasina karşılık, 2B GaN görece daha geniş ve indirekt bir bant aralğına sahiptir. Buna ek olarak 2B GaN daha yüksek Poisson katsayısına sahiptir ve katyondan anyona daha az yük geçişi sergilemektedir. g-GaN icin öngörülen özelliklerini, bu yapı me- talik ya da yarı iletken bir alttaş üzerinde büyütüldüğü takdirde de koruyacağı gösterilmiştir. Özel olarak, g-GaN büyütmek için 3B atomik katmanlı mavi fosforun uygun bir alttaş olacağı öngörülmüştür. Elektronik özelliklerin katman sayısına bağlı olarak kontrol edilebildiği, ve katman sayısı arttıkça bant aralığının azaldığı ve indirekt bant aralığından direkte geçildiği gösterilmiştir. Bu çalismanın nanoelektronik uygulamalarda geniş bir kullanım alanı olacağı düşünülen g-GaN'ın büyütülmesi yönünde yardımcı olması umulmaktadır.

Anahtar sözcükler: İki-boyutlu (2B) malzemeler, galyum nitrür (GaN), ilk prensip hesaplamalar, yoğunluk fonksiyonel teorisi (YFT).

Acknowledgement

First and foremost I wish to thank my supervisor, Dr Engin Durgun, who has supported me throughout these two years during my masters studies with his patience, motivation, guidance, "friendship", and knowledge while allowing me the room to work in my own way.

I would like to thank;

Dr Ethem Aktürk for his trust, help, and guidance both in my undergraduate years and related with my graduate studies.

Prof Salim Çıracı, who needs no description. I consider myself lucky to meet him and work with him, and it has been an honor for me.

My thesis committee members Dr Oğuz Gülseren and Dr Hande Toffoli for their time, kindness, insightful comments, and enlightening questions.

Dr Deniz Keçik related with this study in particular, and Dr Semran İpek for answering all my questions and for her discussions which thought me a lot. And also Sami Bolat for inspiring discussions and his passion in this field.

Finally I thank to coffee producers, and musicians whom songs I have listened during thesis writing, while I prefer to keep my expressions of gratitude to my friends and family for my PhD thesis.

This work was supported by the Scientific and Technological Research Council of Turkey (TUBITAK) under Project No 115F088, and I acknowledge fellowship from TUBITAK under Project number 114F169. The calculations were performed at TUBITAK ULAKBIM, High Performance and Grid Computing Center (TR-Grid e-Infrastructure) and UHEM, National Center for High Performance Computing.

Contents

List of Figures

List of Tables

Chapter 1

Introduction

The replacement of a material with mechanical parts leads to smaller, more efficient, and more accurate devices. The invention of mainspring, basically a "mechanical battery", enabled tower watches, which uses pendulum, shrink to pocket sized ones. Later on using a quartz crystal and a battery led to more accurate and yet smaller ones, and the working principles of a watch was changed. Materials offer lots of different possibilities with their different properties depending on their crystal structure, orientation, constituent atoms, and scales ranging from 3 dimensional bulk structure to 0 dimensional nanoparticles.

It had been argued that 2-dimensional (2D) crystals could not exist [6, 7, 8] until the first 2D material, graphene, was isolated from its layered bulk crystal, graphite, through mechanical exfoliation in 2004 [9]. Graphene is a single layer of carbon atoms (1.1) which bond together such that they form a honeycomb structure. Each carbon atom has sp^2-hybridized orbitals forming σ bonds, and p_z orbitals forming π bonds. These σ bonds are responsible for the strong binding between the carbon atoms in graphene, and the π bonds give rise to van-der-Waals (vdW) interaction between the graphene layers in graphite. Due to these strong bonds within a graphene layer, it is the strongest material known to date having an ultimate tensile strength of 130 GPa and a Young's modulus around 1TPa [10], and the weak vdW interaction between the layers enables easy isolation of layers

from each other. One peculiar property of graphene is that the dispersion relation at the K points of the Brillouin zone is linear (1.1), which enables electrons and holes have zero effective mass. Therefore these electrons and holes near the K points behave like relativistic particles which are called Dirac fermions which can be described by Dirac equation. Moreover it is endowed with other remarkable properties including very high electrical and thermal conductivity [9, 11, 12, 13]. Due to its remarkable properties mentioned above, graphene has been subject to extensive studies, and it is considered as a very promising material to be used in various fields and currently used in many applications including energy storage [14], tarnsparent and elastic electronics [15], optical devices [16], or electrically switchable radar-absorbing surfaces are realized by using large-area graphene capasitors [17]. On the other hand, being a semimetal having zero band gap, the applications in nanoelectronis are limited. The possibility of opening a gap is investigated, however the achieved band gap is very small up to date for desired practical applications like logical circuits at room temperature.

Unique properties of graphene, inevitably, brings a question; Whether the single layers of other Group-IV elements, including silicon which is the "core" material in today's technology, exist? Theoretical studies using first-principles phonon and high temperature molecular dynamics (MD) calculations within Density Functional Theory (DFT), have demonstrated the stability of silicon and germanium in buckled honeycomb structure [18, 19, 20], named as silicene and germanene respectively, which are isovalent with graphene. They both are semimetal with linearly crossing bands at the Fermi level similar to graphene which also has Dirac cones in their electronic structure represented in three dimensions. Even though they do not have a layered bulk structure, silicene and germane also realized experimentally [21, 22, 23]. Considering the effect of silicon in today's technology, if achieved with desired properties, silicene based transistors suggest easier integration compared to other 2D materials for nanoelectronic devices. Although it has lower mobility values when compared to graphene transistors, silicene based transistors are also realized [24]. In search of 2D forms of group-IV elements, going down the row, the "last" one is tin, namely stanene. It has also been synthesized offering a potential topological insulator behaviour in 2D

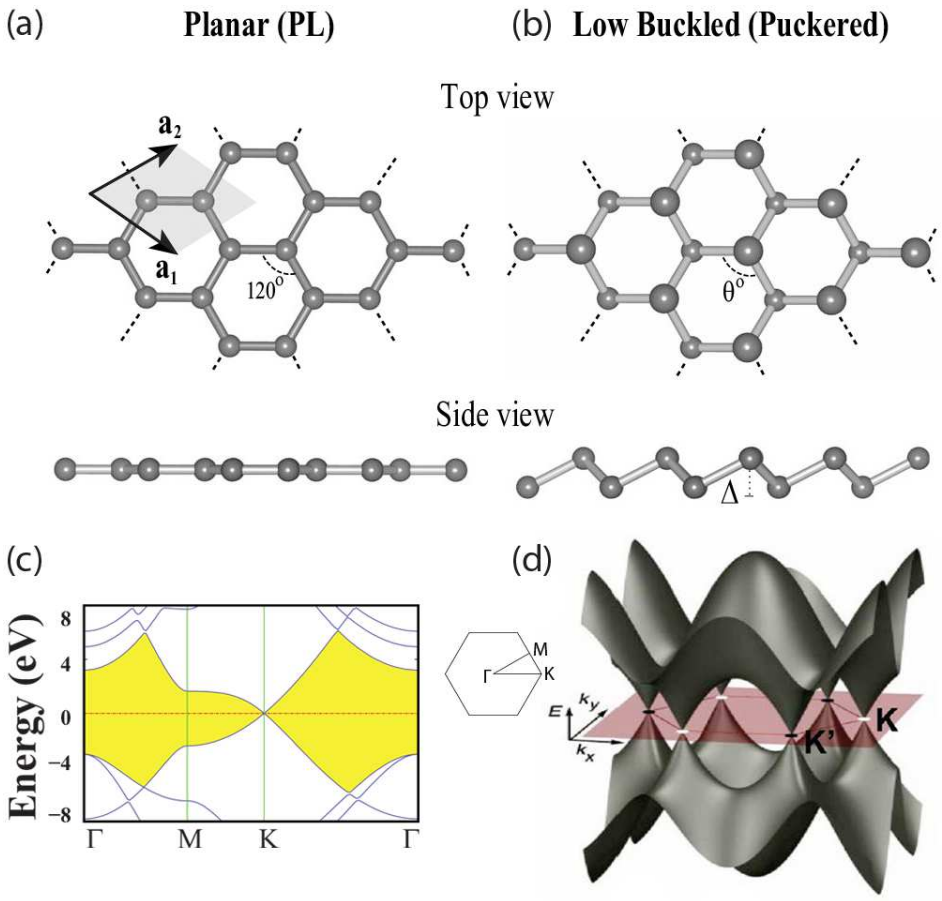

Figure 1.1: Top and side views of two-dimensional (a) planar (b) buckled honeycomb structures. $\mathbf{a}_1$ and $\mathbf{a}_2$ represent lattice vectors, and Δ shows buckling distance.(c) Energy band structure of graphene[1]. (d) Three-dimensional band structure of graphene showing Dirac cones[2].

[25, 26].

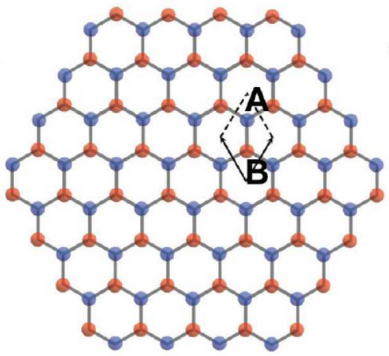

Figure 1.2: Top view of a two-dimensional material having a honeycomb structure composed of two different atoms A and B[2].

Transition metal dichalcogenides[27, 28, 29] (TMDs) are another "family" of 2D materials which presents a stoichiometry in the form MX_2 where M and X correspond to a transition metal and a chalcogenide, respectively. One TMD layer is composed of three atomic layers; one layer of metal atoms sandwiched between two chalcogene atomic layers forming a hexagonal structure, and each M atom is covalently bonded to the nearest X atom. They can be both metallic or semiconducting. The most famous one among them is molybdenum disulfide(MoS_2). Unlike the semimetallic graphene and insulating hexagonal boron nitride(h-BN), single layer of MoS_2[30, 27] is a semiconductor with a natural direct band gap of 1.90eV. Being a semiconductor and getting isolated from its layered bulk structure via mechanical exfoliation, single layer MoS_2 has been subject to extensive research, and has been an exciting candidate for electronics applications.

Another promising material for 2D electronics is phosphorene (group V) which has been mechanically exfoliated from its bulk structure [31, 32],black phosphorous. It is a direct band gap semiconductor like MoS_2, but phosphorene based FETs shows higher carrier mobilities than MoS_2 based counterparts [32]. Motivated with the realization of phospherene, other Group V systems (nitrogene, antimonene, and bismuthene) are also predicted theoretically and all have been found stable above room temperature [33, 34]. Almost continuously, new single layer or few layer materials are synthesized, new properties of them are explored,

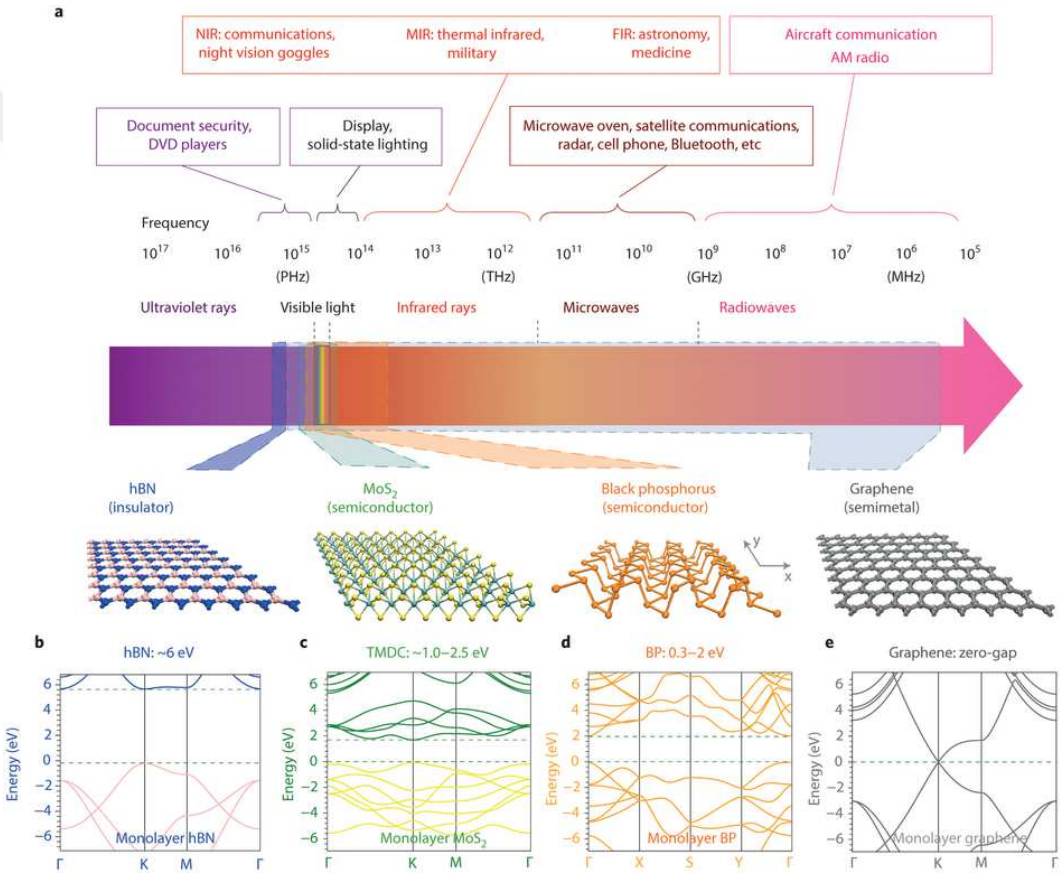

Figure 1.3: (a) Applications that utilize the different spectral ranges in electromagnetic spectrum,and the crystal structures of h-BN, MoS˙2, BP and graphene are shown from left to right. The possible spectral ranges covered by different materials are indicated using coloured polygons. Electronic band structures of (b) single-layer h-BN (c), MoS2 (d), BP, and (e) graphene.[3]

and new applications of them (including proof-of-concept applications) are realized. The research of finding tunable band gap materials and methods continues to succeed the exciting concept, 2D electronics. Different classes of 2D materials and their possible applications are summarized in 1.3

In a couple of theoretical studies, it has been predicted that III-V compounds[1, 35] and also a group II-VI compound,[36] with constituent elements having s^2p^m valence orbitals can form stable, graphene like, single layer (SL) honeycomb structures with 2D hexagonal lattice. Consisting of similar structure with graphene, monolayer hexagonal boron nitride (1.2) (h-BN) sheets have vdW interaction with each other forming layered bulk structure from which single layer h-BN can be exfoliated mechanically [37]. Unlike other semiconducting III-V 2D compounds, h-BN is an insulator [1, 38, 39]. It has a low lattice mismatch with graphene, therefore it has attracted great attention because of the potential to be used as a 2D dielectric material in graphene transistors [40, 41], and found to increase device performance [40]. The second III-nitride to be mentioned here is aluminum nitride (AlN). Earlier, it has been predicted to have stable hexagonal crystal structure (1.2) when it is one atom thick [1], and few-layer form recently realized experimentally via plasma assisted molecular beam epitaxy (MBE) on Ag(111) surface [42]. With its layer and strain dependent tunable properties, 2D h-AlN is a promising material for optoelectronic applications[43].

Being one of the III-V compounds, GaN in wurtzite structure (wz-GaN) has excellent electronic and optical properties which make it an important semiconductor with critical and wide range of technological applications in microwave communications, lasers, detectors, light-emitting diodes in the UV range etc. [44, 45] It has $\sim$3.4 eV direct band gap and exhibits high chemical, thermal and mechanical stability, which is convenient for various applications like nano-electro mechanical systems (NEMS). Additionally, GaN and similar III-V compounds like AlN can form heterostructures with commensurate interfaces, which offer interesting quantum structures in lower dimensionality and display unusual device properties. Besides, 3D GaN crystal can be grown easily by various methods, whereby the fabrication of thin films and heterostructures are achieved. However,

so far a single-layer GaN has not been synthesized yet. In view of the recent advances in growth techniques and experiences developed through the fabrication of GaN thin films, it is expected that the growth of SL honeycomb structure of GaN, i.e. g-GaN can be achieved soon. Given the role of wz-GaN in device technology, the growth of g-GaN would be a real impact in 2D flexible nano-optoelectronics.

Figure 1.4: A prototype laptop power adapter made by Cambridge Electronics using GaN transistors. At 1.5 cubic inches in volume, this is the smallest laptop power adapter ever made.[4].

While the positive phonon frequencies in a previous study[1] indicates stability against small displacements, the stability at high temperature was not assured for g-GaN. Then the main task of this study is firstly to show that g-GaN corresponds to a deep, local minimum on the Born-Oppenheimer surface and hence remains stable at high temperature. Having assured the stability, a comprehensive and comparative study is performed using DFT on 3D wz-GaN and its allotrope in cubic zinc-blende structure, namely zb-GaN, as well as on SL, honeycomb structure together with its multilayers. The main objective is to reveal whether g-GaN can substitute 3D wz-GaN in 2D electronics. It will be clarified how the physical properties, in particular electronic and elastic properties can change as the dimensionality varies from 3D to strictly 2D. In the past, the physical properties, in particular the electronic energy structure of 3D wz-GaN and zb-GaN have been treated by using methods similar to the one used in this study. In a majority of these studies, the calculated band gaps of wz-GaN and zb-GaN

were underestimated by almost 1.7 eV when compared to the experimental values. While this discrepancy between DFT band gap and the experimental value is well known, improving the theoretical predictions of band gaps has been a primary motivation in recent studies including this one. Other objectives of this study have been to explore: (i) Can bilayer, trilayer and periodic multilayer structures be constructed by stacking of g-GaN? (ii) How do their physical properties vary with the number of layers? (iii) Can a suitable substrate be deduced to grow g-GaN and can the properties of g-GaN predicted in this study be modified when it is grown on this substrate?

Important results of this thesis can be summarized as follows: (i) Large discrepancies between experimentally determined fundamental band gap of 3D GaN crystals and DFT results can be overcome by applying corrections to standard techniques based on DFT. Such corrections appear to be necessary also for g-GaN. (ii) Ab-initio MD calculations proved that the honeycomb like structure is maintained stable at temperatures as high as 1000K. (iii) In 2D g-GaN structure, the fundamental band gap increases and becomes indirect. (iv) When grown on semiconducting blue phosphorene, which is lattice matched, the physical properties of the freestanding g-GaN are preserved. In this respect, layered blue phosphorus can be an ideal substrate to grow g-GaN. (v) g-GaN can form stable bilayer, as well as multilayers, where the interlayer binding occurs through chemical and van der Waals (vdW) interaction. The fundamental gap is altered with the number of layers; it decreases and is converted from indirect to direct gap as the number of layer increases. Finally, a 3D layered periodic structure of GaN like graphite can be constructed artificially by stacking of g-GaN.

Chapter 2

Theoretical Background

In principle, properties of a physical system, let us say an atom or a collection of atoms, can be derived by solving the Schrödinger equation. The time-independant many-body Schrödinger equation can be simple written as

$$\widehat{H}\Psi = E\Psi \tag{2.1}$$

where $\widehat{H}$ is the Hamiltonian operator, Ψ is the state function, and E is the eigenvalue of the Hamiltonian corresponding to that particular solution Ψ. The Hamiltonian of a system consisting of a number of nuclei and electrons can be written in a general form as

$$H = \sum_{I=1}^{N} \frac{\overrightarrow{P_I^2}}{2M_I} + \sum_{i=1}^{N_e} \frac{\overrightarrow{p_i^2}}{2m} + \sum_{i>j} \frac{e^2}{|\overrightarrow{r_i} - \overrightarrow{r_j}|} + \sum_{I>J} \frac{Z_I Z_J e^2}{|\overrightarrow{R_I} - \overrightarrow{R_J}|} - \sum_{i,I} \frac{Z_I e^2}{|\overrightarrow{R_I} - \overrightarrow{r_i}|} \tag{2.2}$$

where M_I, Z_I and R_I, $I = 1, ..., N$ correspond to nuclear masses, nuclear charges and nuclear positions of each nuclei, respectively, and m_i and r_i, $i = 1, ..., N$ correspond to electrons masses and electron positions. Each term in the Hamiltonian operator defines kinetic energy of nuclei, kinetic energy of electrons, interaction between electrons, interaction between nuclei, and interaction between neclei and electrons, respectively.

However it is not possible to solve Schrödinger equation for a particular system

except for simple cases like hydrogen atom which is only a two-particle system, or harmonic oscillator, or particle in a box problem. Main problem is 2.2 cannot be decoupled into a set of independent equations because it describes a many-body system in which electrostatic correlation exist between each component. Inevitably approximation methods should be applied.

Taking into account the fact that a nucleus has more than 1800 times the mass of an electron, one can easily say that electrons respond "instantaneously" to a change compared to nuclei. Thus we can split the Hamiltonian into two pieces: nuclear part and electronic part, and solve the electronic part for fixed coordinates of the nuclei. This separation of nuclear part and electronic part into separate problems is known as the Born Oppenheimer approximation [46].

The separated electronic part of the equation having electron wave function is still too complex to solve. An approximation suggested by Hartree postulates that the electron wave function which involves all the electrons can be thought as product of single electron wave functions each of which satisfies single-particle Schrödinger equation in an effective potential [47]. Defining the many-electron wave function as product of single-electron wave functions is known as Hartree product and can be shown as

$$\Psi(\mathbf{R}, \mathbf{r}) = \Pi_i \psi(\mathbf{r}_i) \tag{2.3}$$

and single electron wave function in an effective potential is defined as

$$(-\frac{\hbar^2}{2m}\nabla^2 + V_{eff}^{(i)}(\mathbf{R}, \mathbf{r}))\psi_i(\mathbf{r}) = \epsilon_i \psi_i(\mathbf{r}) \tag{2.4}$$

with

$$V_{eff}^{(i)}(\mathbf{R}, \mathbf{r}) = V(\mathbf{R}, \mathbf{r}) + \int \frac{\sum_{j \neq i}^{N} \rho_j(\mathbf{r}')}{|\mathbf{r} - \mathbf{r}'|} d\mathbf{r}\text{'} \tag{2.5}$$

where

$$\rho_j(\mathbf{r}) = |\psi_j(\mathbf{r})|^2 \tag{2.6}$$

is the electronic density associated with particle j. Effective potential does not include the charge density terms associated with i, in order to prevent self-interaction terms. Thus the energy associated with the Hamiltonian formed with

2.5 is found as

$$E^H = \sum_i^N \varepsilon_n - \frac{1}{2}\int\int \frac{\rho(\mathbf{r})\rho(\mathbf{r}')}{|\mathbf{r}-\mathbf{r}'|} d\mathbf{r}d\mathbf{r}' \tag{2.7}$$

where $1/2$ factor ensures that electron-electron interaction is not counted twice.

The solution of 2.4 is a single-electron wave function. This state function gives electron density which defines the effective potential given in 2.5. But effective potential was required to solve the single-electron wave function in the first place. This situation may seem like a vicious cycle but the solution is to begin with a good guess of trial wave function and then try to minimize the energy by performing iterative calculations. This self-consistency concept will be mentioned below while density functional theory is discussed briefly.

Pauli exclusion principle states that no two identical fermions can be in the same quantum state. This principle requires exchange interaction to be taken into account while dealing with electron wave function. Under these circumstances total electron wave function must be antisymmetric which means that wave function changes sign when two arguments are exchanged as follows:

$$\Psi(1,..,i,..,j,..,N) = -\Psi(1,..,j,..,i,..,N) \tag{2.8}$$

which can be satisfied by a determinant concept

$$\Psi(1,..,i,..,N) = \begin{vmatrix} \psi_1(\mathbf{r_1}) & \dots & \psi_1(\mathbf{r_i}) & \dots & \psi_1(\mathbf{r_N}) \\ \vdots & \ddots & \vdots & \ddots & \vdots \\ \psi_i(\mathbf{r_1}) & \dots & \psi_i(\mathbf{r_i}) & \dots & \psi_i(\mathbf{r_N}) \\ \vdots & \ddots & \vdots & \ddots & \vdots \\ \psi_N(\mathbf{r_1}) & \dots & \psi_N(\mathbf{r_i}) & \dots & \psi_N(\mathbf{r_N}) \end{vmatrix} \tag{2.9}$$

which is known as Slater determinant. Being an improvement of Hartree approximation where electron wavefunction also satisfies Pauli exclusion principle, and known as Hartree-Fock approximation.

2.1 Density Functional Theory

Although Schrödinger equation provides exact solutions of a many-body system, collection of atoms interacting with each other in this case, it is not possible to solve. An alternative approach suggests using electron density rtaher than many-electron wave function, which is known as density functional theory (DFT).

2.1.1 Hohenberg-Kohn Formulation and Kohn-Sham Equations

Density functional theory rests on two fundamental theorems proposed and proved by Hohenberg and Kohn [48].

First theorem states that ***the ground state energy determined by solving Schrödinger equation is a unique functional of the electron density***. One can conclude from this theorem that there is a one-to-one correlation between the ground state density and the ground state properties of the system. But here there is no information about the functional.

Here, not surprisingly, the second theorem, also known as variational principle, appears stating; ***The electron density that minimizes the energy of the overall functional is the true electron density corresponding to the full solution of the Schrödinger equation***. If the functional were known, one could vary the electron density and find the minimum of the functional which correspond to the ground state electron density which is required. On the way to find the functional described by the second theorem, Kohn-Sham equations [49] come to aid.

Following Kohn and Sham, in order to get the right electron density, a set of equations each of which involves a single electron are needed. These equations are known as Kohn-Sham equations and can be expressed as

$$\left[-\frac{h^2}{2m}\nabla^2 + V_{ext}(\mathbf{r}_i) + V_H(\mathbf{r}_i) + V_{XC}(\mathbf{r}_i)\right]\psi_i(\mathbf{r}_i) = \epsilon_i\psi_i(\mathbf{r}_i) \tag{2.10}$$

or in more compact form

$$\left[-\frac{h^2}{2m}\nabla^2 + V_{eff}\right]\psi_i = \epsilon_i\psi_i \tag{2.11}$$

where V_H is the Hartree potential defined as

$$V_H(\mathbf{r}) = e^2 \int d^3r' \frac{n(\mathbf{r}')}{|\mathbf{r} - \mathbf{r}'|} \tag{2.12}$$

and V_{XC} is the potential term which defines exchange-correlation contributions to 2.10.

Let us assume the "problematic" exchange-correlation potential is known. In order to solve the Kohn-Sham equation we need to know the Hartree potential but the definition of Hartree potential involves electron density. To find the electron density, single electron wave functions must be known. And this requires solving the Kohn-Sham equations. This situation seems like a vicious cycle again mentioned above. The solution lies in the iterative (self-consistent) approach: Begin with a trial electron density, solve the Kohn-Sham equations and find the wave functions, and define the new electron density. Compare the previous and the last densities. If they are the "same", then it is done, but if they are "different" then continue iteration.

2.1.2 Exchange-Correlation Functionals

Everything seems settled but the most difficult part still remains: exchange-correlation functional is not known. In order to solve the Kohn-Sham equations, exchange-correlation functional must be specified. Exact derivation of this functional is known only for one case which is the uniform electron gas. Uniformity implies that its electron density is constant in space($n(\mathbf{r}) = cst$). To make use of this for the purpose of defining a valid functional which will provide solutions that represent the properties of real materials, one can define the exchange-correlation potential at a given position to be the exchange-correlation potential of the uniform electron gas as a functional of the electron density at that position as follows:

$$V_{XC}(\mathbf{r}) = V_{XC}^{electron\ gas}[n(\mathbf{r})] \tag{2.13}$$

Since this approximation uses local densities ($n(\mathbf{r})$ at that position) to define $V_{XC}(\mathbf{r})$ is called local density approximation (LDA). Although it seems a "rough" approximation it works well for many systems. Other than LDA, there is another well known approximation which is called general gradient approximation (GGA). This approximation uses both the local electron density and the local gradient of the electron density. Whereas LDA considers uniform electron distribution, GGA considers the evolution of the density as well.Thus GGA functional involves more information about the physical system over LDA, which is a sign of better representation of a real system, but the way in which the local density gradient is included in GGA functional determines the accuracy of that functional for that specific system, and this variability of the approach to the gradient causes creation of different GGA functionals.

2.1.3 Hybrid Functionals

It is well known that DFT using either LDA or GGA methodolgy underestimates the band gap of the semiconducting materials. The Hartree potential which is also involved in Kohn-Sham equations defines the electrostatic interaction between one electron and the electron density to which all the electrons contribute including that one electron interacting with this electron density. That is to say an electron contributes to the electron density from which it is effected. This interaction is nonphysical, and must be eliminated. In the Hartree-Fock method, this interaction energy is totally cancelled by including the exchange term in Hamiltonian. The same cancellation would be also valid for DFT if the exact form of the functional were known. The errors caused by this situation can be partially corrected by using hybrid functionals. The functionals which incorporates exact exchange of some amount is called as hybrid functional [50]. In solving KS equations in plane-wave basis set, screened hybrid functionals [51] are used. This approach divide the exchange interaction into two parts; long-range and short-range parts. The short-range part includes the exact exchange of some amount.

HSE (Heyd-Scuseria-Ernxerhof) exchange-correlation functional [51], one of the widely used hybrid functionals, is constructed by incorporating PBE correlation functional, and Hartree-Fock exchange functional with a mixing parameter of 1/4 and 0.2 screening parameter for screened Coulomb potential in the short range Hartree-Fock exchange functional, and the remaining 3/4 part of the exchange functional comes from PBE.

$$E_X^{HSE}C = \alpha E_X^{HF\ short\ range} + (1-\alpha)E_X^{PBE\ short\ range}(\gamma) + E_X^{HF\ long\ range}(\gamma) + E_C^{PBE} \tag{2.14}$$

where α is the mixting parameter, and γ is the screening parameter.

2.1.4 Van der Waals Interaction

Van der Waals interaction is a very weak interaction compared to covalent bonding or ionic bonding, but still very important for materials. In order to define the properties of a layered material, i.e. graphite, layered h-BN, the effect of this interaction should be modelled accurately. DFT has a limitation in calculating the weak van der Waals interactions because the approximations made by exchange-correlation functionals (LDA, GGA, or hybrid functionals) are not able to describe long-range electron correlation [52]. The solution is to add a correction energy to the result of Kohn-Sham equations. There are various methods which calculates the correction in different ways, and among them DFT-D2 method of Grimme [53] in VASP is used in this study.

2.1.5 Plane Waves and k-point Sampling

The systems in this study consist of atoms in periodic arrangement. If Schrödinger equation is applied to a periodic system, the solutions which are wave functions must satisfy a property known as Bloch's theorem. This theorem states that the solution of Schr"odinger equation applied to a periodic structure can be written as a sum the terms with the form

$$\psi_k(\mathbf{r}) = e^{i\mathbf{k}.\mathbf{r}} u_k(\mathbf{r}) \tag{2.15}$$

where $u_i(\mathbf{r})$ has the same periodicity with the crystal lattice satisfying the condition $u_i(\mathbf{r}) = u_i(\mathbf{r}+\mathbf{T})$. Here $\mathbf{T}$ is the translation vector of that lattice.

In the case of Kohn-Sahm equations Bloch's theorem still applies and the single electron wave-functions are in the form of Bloch functions expressed as in 2.15. Using a basis set consisting of reciprocal lattice vectors of the crystal, electronic wave functions can be written as a sum of plane waves

$$\psi_i(\mathbf{r}) = \sum_G a_{i,k+G} e^{i(\mathbf{k}+\mathbf{G})\mathbf{r}} \tag{2.16}$$

Integrations over $\mathbf{k}$ requires infinite number of $\mathbf{k}$-points in Brilluoin zone(BZ). But it is possible to represent the reciprocal space with a finite number of $\mathbf{k}$-points which is required or numerical analysis. There are several methods, i.e. Monkhorst-Pack[54], for calculations at specified $\mathbf{k}$-points in the BZ with enough accuracy. The accuracy of a calculation can be determined by the number of $\mathbf{k}$-points used, but the computational burden increases as well.

As discussed above, electron wave functions can be extended in terms of plane wave basis sets (2.16), but evaluating the solution involves infinite number of summations. These functions have solutions with kinetic energies $E = (\hbar^2/2m)|\mathbf{k}+\mathbf{G}|^2$. Luckily the solutions with lower kinetic energies are more important than the higher ones. So it is possible to truncate the infinite sum by using a particular cutoff energy $E_{cut} = (\hbar^2/2m)G_{cut}^2$.

2.2 Computational Parameters used in the calculations

In this thesis, first-principles calculations were performed in order to investigate the ground state properties of bulk and 2D g-GaN, within spin-polarized

density functional theory (DFT). The projector-augmented-wave potentials (PAW) formalism [55] implemented in the Vienna ab-initio simulation package (VASP)[56, 57, 58, 59] is used. The electron exchange and correlation potential was described by the Perdew-Burke-Ernzerhof (PBE) form within the generalized gradient approximation (GGA), with *d*-electrons also taken into account (GGA-d XC potential).[60, 61] The plane-wave basis set was defined by an energy cutoff at 520 eV for all calculations. Moreover, the van der Waals interactions were accounted for the layered structures.[62] Atomic positions were optimized using the conjugate gradient (CG) method; the total energy and atomic forces are minimized with an energy difference between the sequential steps set to 10^{-5} eV for convergence. The maximum allowed force on each atom and Gaussian smearing factor were taken as 0.05 eV/Å and 0.05 eV, respectively. A Γ centered $35\times35\times1$ mesh was used for the Brillouin zone integrations of the primitive unit cell. In order to avoid spurious interactions between the periodic images, a supercell with $\sim$ 20 Å vacuum space was adopted. The cohesive energies of 3D and 2D GaN allotropes are calculated from the expression, $E_c = E_T[Ga] + E_T[N] - E_T[GaN]$ in terms of the total energies, $E_T[Ga]$ and $E_T[N]$ of free Ga and N atoms and the optimized total energy, $E_T[GaN]$ of a specific allotrope. The higher the positive E_c, the stronger is the binding. An interionic charge transfer analysis between Ga and N was carried out for the bulk and g-GaN, using the Bader charge analysis method.[5]

In addition to ab-initio phonon calculations,[63, 64] the stability of the structures were tested at high temperatures by ab-initio molecular dynamics (MD) calculations using two different approaches. In the first one, Nosé thermostat[65] was used and Newton's equations were integrated through Verlet algorithm with a time step of 1 fs. In the second one, the velocities are scaled at each time step in order to keep the temperature constant.

Subsequent to the standard-DFT results, hybrid functionals (HSE06)[66, 51, 67] and quasiparticle (QP) G_0W_0 corrections[68, 69, 70], where G and W were iterated once, were undertaken in order to obtain the corrected band structures of bulk and g-GaN.

Chapter 3

Results

3.1 3D GaN Crystals

The thermodynamically stable phase of 3D GaN crystal has wurtzite structure, which corresponds to a global minimum. As for zb-GaN, it can form in the epitaxial growth of thin films on (011) planes of the cubic substrates[45] and hence has a slightly lower cohesive energy relative to wz-GaN.

3.1.1 Crystal Structure and Energetics

wz-GaN is constructed from two interpenetrating hexagonal close packed lattices, each having two of each constituent atoms, Ga or N. The structure has $P63mc$ space group symmetry, and lattice constants a=b and c. zb-GaN consists of two interpenetrating fcc lattices each having four of the two atoms at the lattice points. The cubic structure has $F\bar{4}3m$ space group. Both allotropes have tetrahedral coordination for the first nearest neighbors, but differ in the second nearest neighbor coordination.

In the present study, we carried out structure optimization calculations of

wz-GaN and zb-GaN crystal with GGA (using only $4s$ and $4p$ valence orbitals), GGA+d (including also $3d$ orbitals), GGA-GW and GGA+d-GW potentials; however we prefer to display and tabulate the results only given by GGA+d potential throughout the paper, due to the reliable values given by this functional. In Fig. 3.1 we present atomic configurations of wz-GaN and zb-GaN in their conventional cells, which were optimized through GGA+d calculations.

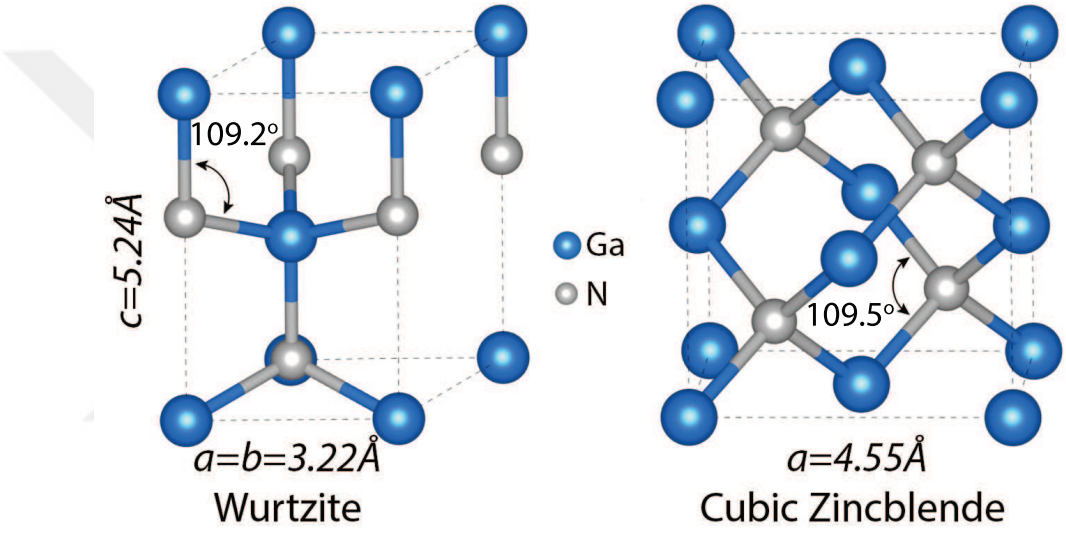

Figure 3.1: Optimized atomic structures of wz-GaN and zb-GaN in their hexagonal and cubic conventional cells, respectively. Lattice constants and bond angles are indicated. Larger (blue) and smaller (gray) balls stand for Ga and N atoms.

For each optimized structure, we calculated the lattice constants, Ga-N bond length d, cohesive energy per Ga-N pair E_c, bulk modulus B, charge transfer from cation to anion Q_b^*, Born effective charge Z^*, and direct band gap between valence and conduction bands E_{G-d}. Our results are listed in Table 3.1 for wz-GaN and in Table 3.2 for zb-GaN. Present calculated values can be compared with values calculated by previous theoretical studies and measured experimentally presented in the same tables.

While the previous LDA calculations provides overbinding, predicting a=3.17 Å and c=5.15 Å, the corresponding experimental values were measured as a=3.19 Å and c=5.19 Å. Apparently, lattice constants of wz-GaN are underestimated by LDA calculations. The present GGA+d calculations predict a=3.22 Å and c=5.24 Å. Also the experimental value of the cohesive energy, 9.06 eV/GaN pair is

	a (Å)	c (Å)	c/a	d (Å)	E_c (eV/GaN)	B (GPa)	ν (%)	Q_b^* (e)	Z^* (e)	E_{G-d} (eV)
GGA+d	3.22	5.24	1.63	1.97	8.76	171	0.18	1.54	2.63	1.71
HSE06 (α=0.25/0.35)	-	-	-	-	-	-	-	-	-	2.96/3.48
G_0W_0	-	-	-	-	-	-	-	-	-	3.03
LDA/GGA[71]	3.16/3.22	5.15/5.24	1.63	-	-	-	-	-	-	2.12/1.74
LDA[72]	3.14	-	1.63	-	-	215	-	-	2.64	-
LDA[73]	3.20	-	1.63	-	-	-	-	-	2.72	-
LDA[74]	3.15	-	1.63	-	-	195	-	-	-	-
GGA[75]	3.19	-	-	-	-	-	-	-	-	1.83
LDA/HSE[76]	3.15/3.18	5.14/5.17	1.63	-	-	-	-	-	2.58/2.64	-
LDA@FP-LAPW[77]	3.17	5.15	1.63	-	-	207	-	-	-	2.22
HSE06[78]	3.20	5.20	1.63	-	-	-	-	-	-	3.21
HSE06 (α=0.25/0.30)[71]	3.18/3.17	5.17/5.16	1.63	-	-	-	-	-	-	3.27/3.48
G_0W_0@OEP$_x$(cLDA)[79]	3.19	5.19	1.63	-	-	-	-	-	-	3.24
Expt.[75, 80, 81, 82, 83, 84, 85, 86, 87]	3.19	5.19	1.63	-	9.06	188,195,205,237,245	0.20	-	2.65	3.40-3.50

Table 3.1: Lattice constants $a = b$ and c; c/a ratio; Ga-N bond length d, cohesive energy E_c per Ga-N pair; bulk modulus B, Poisson's ratio ν, charge transfer Q_b^* from cation to anion through Bader analysis[5], Born effective charges Z^*, and direct band gap E_{G-d} of wz-GaN crystal calculated by using PBE, HSE06 (with different mixing parameters α) and G_0W_0 approaches. For the sake of comparison, values obtained from the previous theoretical studies and experiments are also included.

predicted here as E_c=8.76 eV/GaN pair. As for the bulk modulus, the predicted value of 171 GPa is lower than the experimentally measured values between 188-245 GPa. Furthermore, Bader charge analysis[5] reveals that charge transfer Q_b^* from Ga to N atoms was at a value of 1.54 electrons.

	a (Å)	d (Å)	E_c (eV/GaN)	B (GPa)	ν (%)	Q_b^* (e)	Z^* (e)	E_{G-d} (eV)
GGA+d	4.55	1.97	8.75	170	0.34	1.52	2.68	1.55
HSE06 (α=0.25/0.35)	-	-	-	-	-	-	-	2.74/3.30
G_0W_0	-	-	-	-	-	-	-	2.85
LDA[74]	4.46	-	-	183	-	-	-	-
LDA[72]	4.45	-	-	207	-	-	2.65	-
GGA[88]	4.56	-	-	-	-	-	-	1.66
G_0W_0@LDA[89, 90, 91]	4.5	-	-	-	-	-	-	2.79,2.88,3.09
Expt.[81, 92, 93, 94]	4.54,4.50	-	8.90	185-190	0.37	-	-	3.30

Table 3.2: Cubic lattice constant a; Ga-N bond length d, cohesive energy E_c per Ga-N pair; bulk modulus B, Poisson's ratio ν, charge transfer Q_b^* from cation to anion obtained by Bader analysis[5], Born effective charge Z^*, and direct band gap E_{G-d} calculated by PBE, HSE06 (with different mixing parameters α) and G_0W_0. For the sake of comparison values obtained from the previous theoretical studies and experiments are also included.

For zb-GaN, GGA+d calculations provide best predictions; calculated value of a=4.55 Å for the experimental lattice constant of a=4.54 Å. As expected, the cohesive energy of zb-GaN calculated as E_c=8.75 eV/pair is slightly smaller than

that of wz-GaN, which can be compared with the experimental value measured as 8.90 eV/GaN pair.[94] The bulk modulus, which is calculated to be B=170 GPa is in good agreement with the experimental values reported as 185-190 GPa.[92, 93]

3.1.2 Electronic Structure of 3D GaN Crystals

In a simple tight binding picture of the Bond Orbital Model[95], the cation Ga having $4s^2 4p^1$ and the anion N having $2s^2 2p^3$ valence orbitals each form four sp^3 hybrid orbitals, $|h_c>$ and $|h_a>$, in the tetrahedral directions. The sp^3 hybrid orbital of N has lower energy than the sp^3 hybrid orbital of Ga, namely $E_{|h_c>} > E_{|h_a>}$. When combined to form bond orbitals $\Psi_b >= (|h_c> + |h_a>)/\sqrt{2}$ along four tetrahedrally coordinated bonds, charge is transferred from cation to anion attributing some polar character to covalent bond orbitals. As a result, directional bond orbitals carry both polarity and covalency. According to the Bond Orbital Model, GaN bonds have the polarity α=0.62. In compliance with this analysis, the top of the valence band is dominated by N-2p orbital states. Eight electrons per Ga-N pair and energy difference of $E_{|h_a>}$ and $E_{|h_c>}$ dictate a wide band gap of 3D GaN crystals. With the guidance of this simple analysis, we now examine the calculated electronic band structure of 3D GaN crystals.

In Fig. 3.2 we present the electronic band structure of wz-GaN, which was calculated within GGA approximated using PBE along major symmetry directions. It is a direct band gap semiconductor with E_{G-d}=1.71 eV, which is underestimated by 1.7 eV with respect to the reported experimental values, in the range of 3.40-3.50 eV. Our prediction agrees with the previous calculations within GGA approximation,[71] but 0.4 eV smaller than that of LDA.[71] Present and previous GGA calculations, as well as other previous calculations are known to underestimate the fundamental band gap. Here we apply corrections to present PBE values by using HSE06 and quasiparticle GW methods. After HSE06 correction, the direct band gap of wz-GaN increases to 2.96 eV (and even to 3.48 eV when exchange parameter α=0.35), yet remains $\sim$ 0.44 eV below the experimental value. The GW correction slightly opens up the band gap further to 3.03 eV, which is

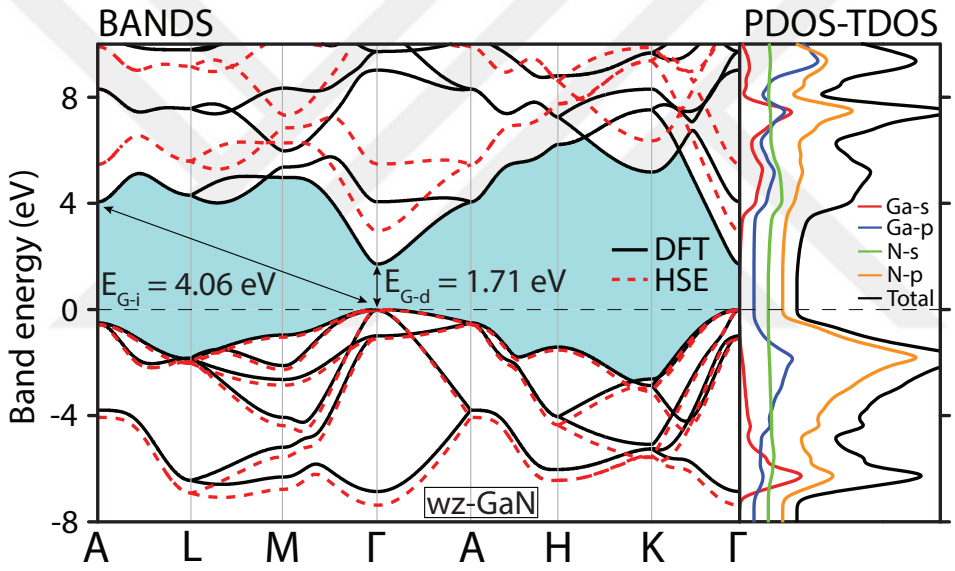

Figure 3.2: Electronic energy band structure of wz-GaN calculated by PBE. The total (TDOS) and partial (PDOS) densities of states projected to valence orbitals are slightly shifted for clarity. The bands after the HSE corrections are shown by the dashed lines. The fundamental band gap of PBE calculations are shaded. The zero of energy is taken at the top of the valence band at the center of the Brillouin zone.

still $\sim$ 0.37 eV smaller than the experimental gap.

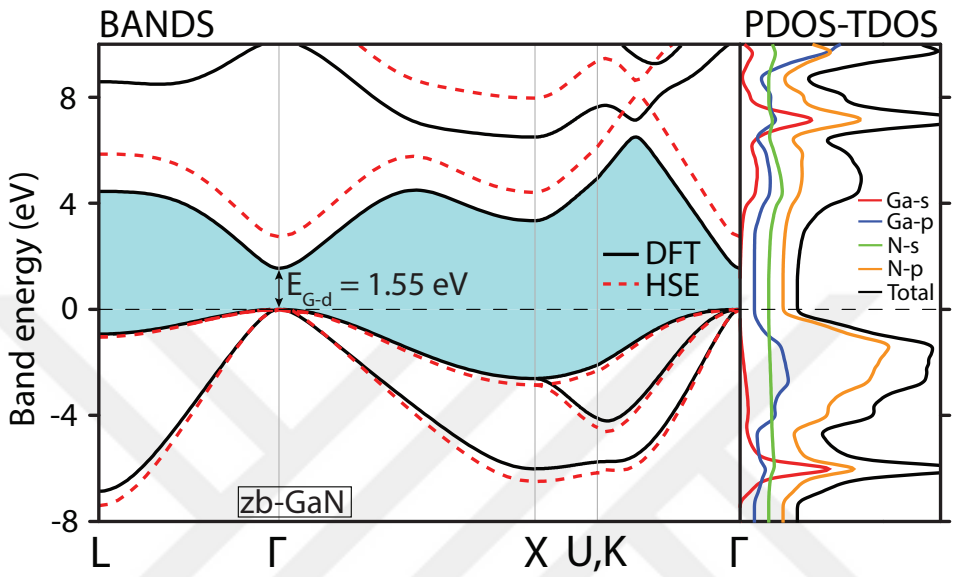

Figure 3.3: Electronic energy band structure of zb-GaN calculated by PBE. TDOS and PDOSs projected to valence orbitals are shifted for clarity. The bands after the HSE corrections are shown by the dashed lines. The fundamental band gap of PBE calculations are shaded. The zero of energy is taken at the top of the valence band at the center of the Brillouin zone.

The electronic energy structure of zb-GaN calculated by PBE is presented in Fig. 3.3. Similar to wz-GaN, zb-GaN is a direct band gap semiconductor with PBE band gap E_{G-d}= 1.55 eV, which is 1.75 eV smaller than the experimentally measured values averaged at 3.30 eV. After HSE06 corrections the calculated value raises to 2.74 eV, yet it is $\sim$ 0.56 eV smaller than experimental values. The G_0W_0 correction opens up the band gap further to 2.85 eV, which is still $\sim$ 0.45 eV smaller than the experimental gap. Nonetheless, fundamental band gaps of both wz-GaN and zb-GaN can be further closed by HSE06 by tuning the exchange parameter α as 0.35, to 3.48 eV and 3.30 eV, respectively.

3.2 2D g-GaN

Using LDA approximation within DFT, the earlier study addressing the question whether IV-IV elemental and III-V and II-VI compound semiconductors can form stable 2D crystalline structures, found that GaN can form a stable, planar, single-layer, honeycomb structure.[1, 35, 36] In the present paper, we name this structure as g-GaN and we first examine its stability, which was proven earlier by phonon calculations.[1] Here, we repeat phonon frequency calculations using GGA and perform also finite temperature MD calculations in order to assure that the equilibrium structure is not a shallow minimum in the Born-Oppenheimer surface. Furthermore, we investigate the properties of g-GaN by using different methods within DFT and apply HSE06 corrections to the fundamental band gap. In doing that, we are able to provide a consistent comparison with the 3D crystals to reveal the effect of the dimensionality.

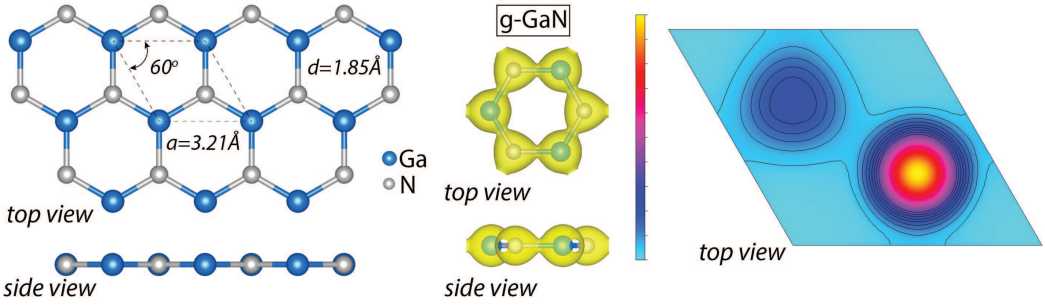

Figure 3.4: Left: Top and side views of the optimized atomic structure of g-GaN. 2D hexagonal primitive unit cell is delineated by dashed lines. The lattice constants a=b and Ga-N bond length are indicated. Large (blue) and relatively smaller (gray) balls denote Ga and N atoms, respectively. Middle: Isosurfaces of the total charge density of the hexagon. Right: Charge density contour plots of Ga-N bond in a horizontal plane passing through Ga-N bond and corresponding color scale. Bond charge of σ-bond is shown.

3.2.1 Structure, Energetics and Mechanical Properties

In g-GaN structure, Ga-sp^2 and N-sp^2 hybrid orbitals form σ-bonds along Ga-N bonds arranged as a hexagon. Due to the planar sp^2 bonding, the bond angle

	a (Å)	d (Å)	E_c (eV/GaN)	C (N/m)	ν (%)	Q_b^* (e)	Z^* (e)	E_{G-i} (eV)
GGA+d	3.21	1.85	8.04	109.8	0.43	1.50	3.08	2.16
HSE06	-	-	-	-	-	-	-	3.42
G_0W_0	-	-	-	-	-	-	-	4.55
LDA[1]	3.20	1.85	12.74	110	0.48	1.70	-	2.27 (GW_0: 5.0)
LDA[96]	3.21	1.85	-	109.4	0.43	-	-	-
LDA[97]	-	1.85	8.38	-	-	-	-	2.17
GGA[98]	-	1.87	8.06	-	-	-	-	1.87 (GW_0: 4.14)
G_0W_0[99]	3.17	-	-	-	-	-	-	4.27 (LDA: 2.36)
PBE/HSE/G_0W_0[100]	3.25	-	-	-	-	1.34	3.23	3.23 (HSE06)/4.00 (G_0W_0)

Table 3.3: Optimized lattice constant a; Ga-N bond length d, cohesive energy E_c per Ga-N pair; in-plane stiffness C, Poisson's ratio ν, charge transfer Q_b^* from Ga to N, Born effective charge Z^*, and indirect band gap E_{G-i} of g-GaN.

between Ga-N bonds is 120^o. In addition to three sp^2 hybrid orbitals of each constituents, Ga and N, their p_z orbitals are perpendicular to the plane of g-GaN. While the σ-bonds attain the strength of g-GaN, the π-bonds between nearest Ga-p_z and N-p_z orbitals maintain the planar geometry of g-GaN. It is known that graphene like compounds are not buckled but are rather planar, if one of the constituents is from the first row of the Periodic Table, like graphene, BN, BP and AlN monolayers with honeycomb structure. Due to the electronic charge transfer from Ga to N, in addition to σ- and π-bonding, an ionic bonding with Madelung energy contributes to the cohesive energy.

The atomic structure of g-GaN was optimized by using the CG method. The equilibrium structure of free standing g-GaN is planar honeycomb structure with 2D hexagonal lattice. The optimized atomic structure together with the primitive cell and its lattice constants is shown in Fig. 3.4. In the same figure, the schematic description of the bonding in compliance with the above discussion is presented. Charge density contour plots of Ga-N bond in a horizontal plane (in the atomic plane of g-GaN) is also shown. The isosurfaces of the total charge density mimic the electron distribution over the hexagons, where Ga and N atoms are alternatingly placed at the corners. It is noted that Ga-N bonds in 3D wz(zb)-GaN, which is constructed from tetrahedrally coordinated sp^3 hybrid orbitals is 0.12 Å longer than the Ga-N bonds of g-GaN constructed from planar sp^2 hybrid orbitals + p_z orbitals. This indicates that Ga-N bonds in g-GaN is stronger than those in wz(zb)-GaN. Despite the stronger bonding in planar g-GaN, the cohesive

energy of 3D wz-GaN crystal, which is four-fold coordinated is 0.70 eV higher than that of g-GaN. Accordingly, g-GaN corresponds to a local minimum in the Born-Oppenheimer surface.

Lattice constants a=b, bond length d, cohesive energy E_c, in-plane stiffness C, charge transfer, Born effective charge values and fundamental band gaps E_G calculated by different methods are presented in Table 3.3. In the same Table, we included results of the previous studies for the sake of comparison.

For g-GaN, our PBE calculation predicts a and d values (3.21 and 1.85 Å, respectively) which are in good agreement with previous theoretical results.[1, 96] While cohesive energy per GaN pair is generally overestimated by LDA calculation, values of in-plane stiffness and Poisson's ratio agree better with previous LDA calculation.[1] Finally, Bader analysis yielding a charge transfer of 1.5 electrons from Ga to N indicates significant ionic contribution in the binding.

3.2.2 Stability: Phonon Spectra and MD Simulations

Even if the structure optimization by CG method indicates the equilibrium structure, it is not necessarily stable under the displacements of atoms in g-GaN. In order to check whether the free-standing g-GaN in honeycomb structure remains stable under the displacements of the constituent atoms, we carry out the calculations of the frequencies of crystal vibrations and determine the phonon frequency spectrum. It is well known that if the vibration frequency of specific modes, $\Omega(\mathbf{k})$ were imaginary, the corresponding displacements would result in an instability, since displacement cannot be restored. In Fig. 3.5(a), the calculated frequencies of phonon modes are positive and indicate stability. The phonon dispersions calculated here are similar to those calculated earlier by using LDA,[1] except for some shifts of the optical branches.

Although the calculated frequencies of the phonon modes are all positive, instabilities can be induced through thermal excitations. This situation occurs when the local minimum of a given phase is shallow and the structure dissociates

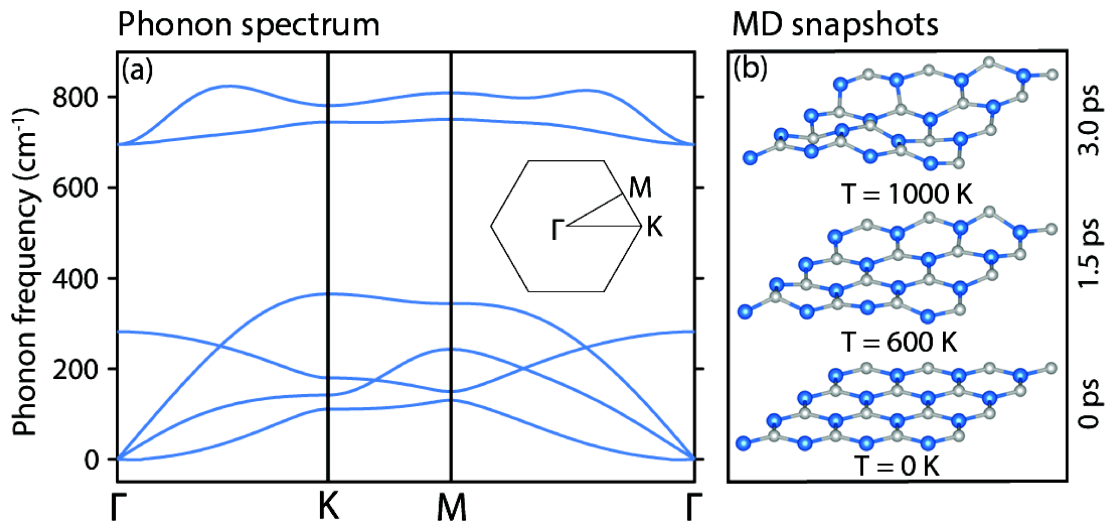

Figure 3.5: (a) Calculated phonon dispersion curves, Ω versus $\mathbf{k}$, along major symmetry directions of the Brillouin zone shown by the inset. (b) Snapshots of the atomic configurations in MD simulations at 0K, 600K and 1000K, in which honeycomb like structures are maintained.

at low temperatures. In order to show that g-GaN can survive at high temperatures and is suitable for technological applications above the room temperature, we carried out ab-initio finite temperature calculations in the temperature range from 0K to 1000K. The honeycomb structure did not dissociate even after 3 picoseconds simulation at 1000K. This indicates that g-GaN is rather stable in a deep minimum on the BO surface and hence devices fabricated from g-GaN can sustain operations above the room temperature. In Fig. 3.5(b) we present snapshots of the atomic configurations obtained from the MD simulations at different temperatures.

3.2.3 Electronic Structure

Since antibonding π^*-bond is separated from π-bond by a significant energy, the π and π^*-bands derived from these bonds open a significant band gap. Accordingly, g-GaN is a nonmagnetic, wide band gap semiconductor. In Fig. 3.6(a) and (b), the electronic energy band structure of g-GaN in the symmetry directions of the hexagonal Brillouin zone, as well as the corresponding total (TDOS) and orbital

projected (PDOS) densities of states are shown. While the maximum of the valence band occurs at the K-point, minimum conduction band appears at the Γ-point. Accordingly, the energy bands calculated by PBE marks an indirect band gap from K- to Γ-point, E_{G-i}=2.16 eV. This is a dramatic deviation from the bulk 3D wz(zb)-GaN, which has a PBE direct band gap of E_{G-d}=1.71. Apparently, the fundamental band gap increased by 0.45 eV as one goes from 3D to monolayer 2D. While the lowest conduction band near the center of the Brillouin zone is derived from the Ga-p_z orbitals, the flat band at maximum of the valence band along K-M direction originates from the N-p_z orbital states. Further to the PBE calculations of the band structure, we applied corrections by using HSE06 and G_0W_0 methods. The corrected band gaps are shown in Fig. 3.6. The indirect PBE band gap increased to 3.42 eV after the HSE06 correction. This corresponds to a correction of 1.26 eV. On the other hand, the correction induced by the G_0W_0 method is larger than that of HSE06 method by nearly 1 eV, revealing a band gap of 4.55 eV. Spin-orbit coupling (SOC) at the top of the valence band at the Γ-point leads to the splitting of the degenerate bands by only 11 meV.

The response of the conduction and valence bands to the applied strain ϵ, and the resulting changes of the fundamental gap is of interest from the fabrication of devices operating under strain. Here we examined the effect of the strain on the fundamental band gap of g-GaN. Within PBE calculations, the band gap of g-GaN was found to monotonically decrease from 2.16 eV to 0.21 eV as going from ϵ=0 to ϵ=10%. Furthermore, the gap seemed to close and lead to a metallic band structure when biaxial tensile strain was further increased, up to 16%. The shifts of the conduction and valence bands under strain and the variation of the fundamental band gap is shown in Fig. 3.7(a) and (b), respectively. This is an important result predicting dramatic changes in the electronic structure with applied strain, once $\epsilon_x = \epsilon_y \leq 10\%$ is affordable in g-GaN system.

As for TDOS and orbital projected PDOS, one also finds modifications by going from 3D to 2D. In particular, flattening of the bands near the edge of the conduction band gives rise to strong peaks in TDOS and PDOS.

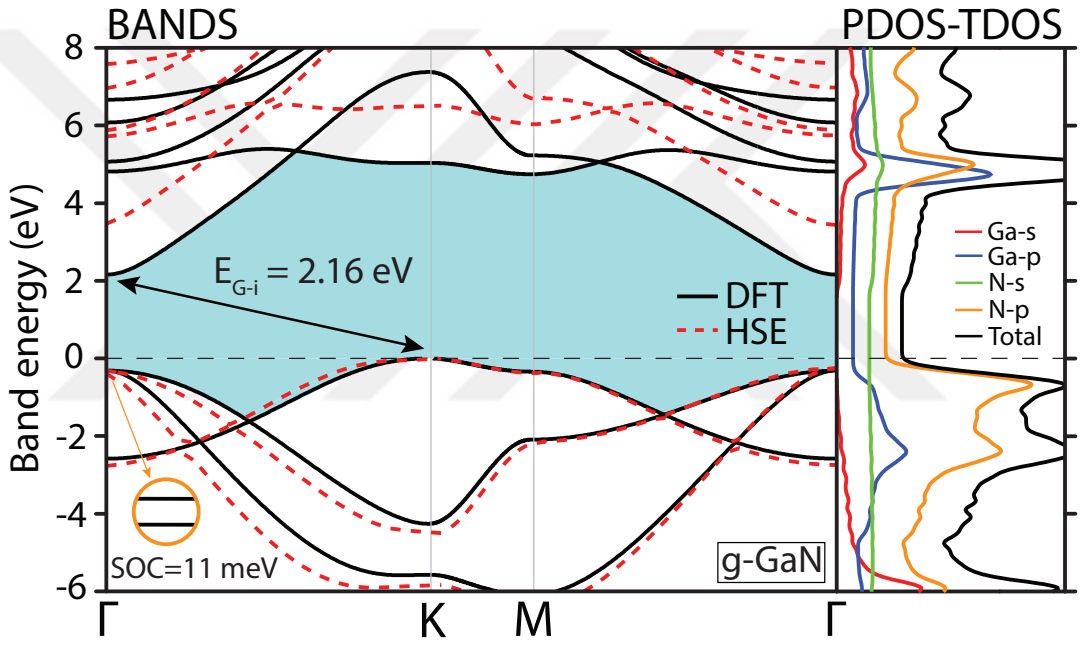

Figure 3.6: Electronic energy band structure of the optimized structure of g-GaN is presented along the symmetry directions of the Brillouin zone. Zero of energy is set to the top of the valence band. Fundamental band gap between conduction and valence bands are shaded and indirect band gap E_{G-i} is indicated. The splitting of the degenerate bands at the top of the valance band at the Γ-point due to spin-orbit coupling is shown by the inset. PBE bands corrected by the HSE06 method are shown by the dashed lines.

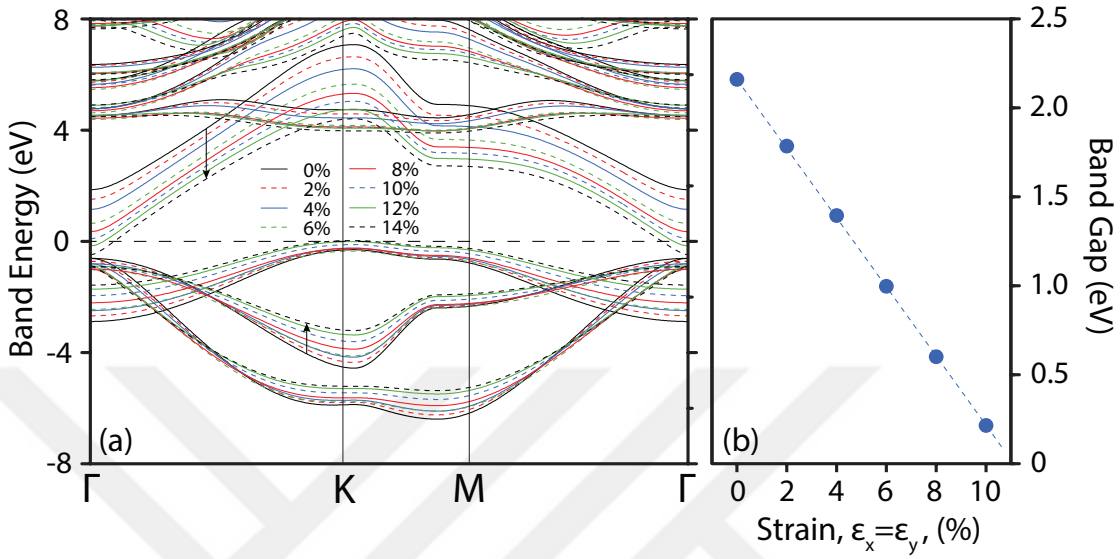

Figure 3.7: (a) Variation of the energy bands of g-GaN near the fundamental band gap under applied biaxial strain $\epsilon_x = \epsilon_y = \epsilon$. (b) Variation of the minimum indirect band gap between Γ and K-points with applied strain

3.2.4 g-GaN on Substrates

Since 3D layered GaN does not exist in nature, the freestanding g-GaN cannot be exfoliated; it should be grown on a substrate. Under these circumstances, the grown overlayer and substrate can be strong and hence the properties calculated for SL g-GaN undergo significant modifications. Here we examined the properties of g-GaN overlayer grown on two different substrates. These are metallic Al(111) surface and semiconducting blue phosphorene. Our models of g-GaN+substrate are presented in Fig. 3.8.

Al(111) surface is rather reactive and hence can establish strong interactions with the g-GaN overlayer. In this respect, Al(111) surface is a stringent test substrate. The Al(111) surface is represented by an Al(111) slab consisting of four Al(111) planes. Since Al(111) surface is not lattice matched to g-GaN, we elongated the Al(111) lattice by 15%. This allows us to treat the g-GaN+substrate system using periodic boundary conditions. Since the electronic

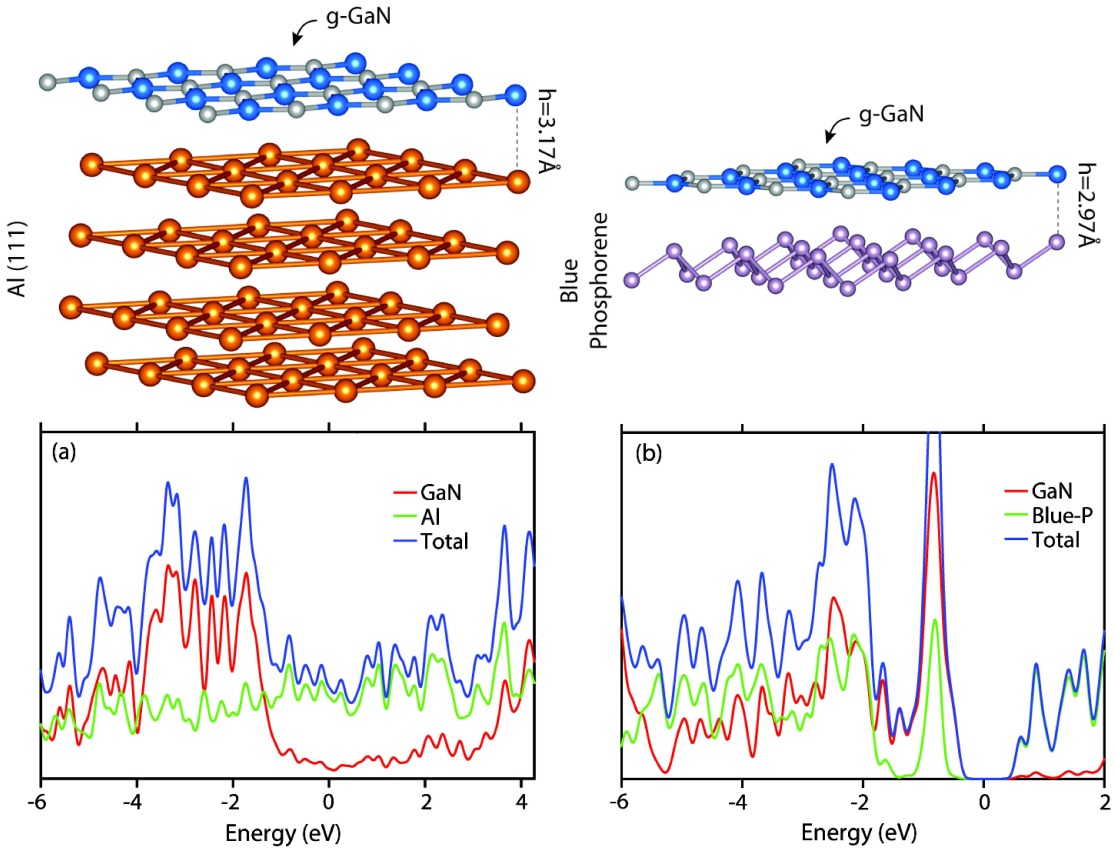

Figure 3.8: (a) Optimized atomic structure of g-GaN overlayer on Al(111) slab represented by four Al(111) atomic planes. Calculated total and local densities of states on the overlayer as well as on Al(111) slab. (b) Optimized atomic structure of g-GaN overlayer on a SL blue phosphorene. Calculated total and local densities of states on the overlayer as well as on SL blue phosphorene.

density of Al(111) is increased upon compression, the reactivity of Al(111) surface can increase to enhance overlayer-substrate interaction. This way our test is realized in even more severe conditions. The effect of Al(111) substrate on g-GaN is analyzed by determining the height of g-GaN from the substrate and by calculating the density of states localized on the overlayer. In Fig. 3.8(a), the optimized height h=3.17 Å, which is larger than the sum of the covalent atomic radii of either $r_{Ga}+r_N$=1.76 Å or r_N+r_{Al}=1.76 Å.[101] The common Fermi level is shifted up by $\sim$ 1 eV from the top of the valence band of g-GaN. The density of states projected onto the g-GaN overlayer is reminiscent of the state density presented in Fig. 3.6 with peaks -1 eV $<$ E $<$ -2 eV and -3 eV $<$ E $<$ -4 eV. Low densities of states in the gap region of g-GaN for energies -1 eV $<$ E $<$ 1.5 eV is partly due to the numerical accuracy and weak substrate-overlayer interaction.

Interestingly, blue phosphorene, i.e. SL buckled honeycomb structure of phosphorus, is nearly lattice matched to g-GaN and hence is an ideal substrate to examine substrate-overlayer interaction. While we consider a single layer of blue phosphorene in order to examine its interaction with g-GaN, the same interaction with the multilayer phosphorene or layered 3D blue phosphorus is not expected to change in any essential manner owing to the weak vdW interlayer interaction within phosphorene. However, because of the semiconducting surface and its lattice constants nearly matching to g-GaN, 3D layered blue phosphorene appears to be an ideal substrate to grow single and multilayer structures of g-GaN. In Fig. 3.6(b), the height of the g-GaN overlayer from blue phosphorene surface is h=2.97 Å, which is rather large and larger than the sums of covalent radii $r_{Ga}+r_P$=2.36 Å. The density of states projected onto g-GaN is similar to that in Fig. 3.6 with the peaks at $\sim$-1 eV, -2.5 eV and -6 eV. The fundamental band gap of the g-GaN+phosphorene system partly overlaps with that of g-GaN, whereas the conduction bands of blue phosphorene occur in the upper energy region of g-GaN overlayer. Briefly the density of states analysis suggests that the interaction between overlayer g-GaN and the underlying blue phosphorene is minute and does not allow any significant modification of the electronic structure of the freestanding g-GaN.

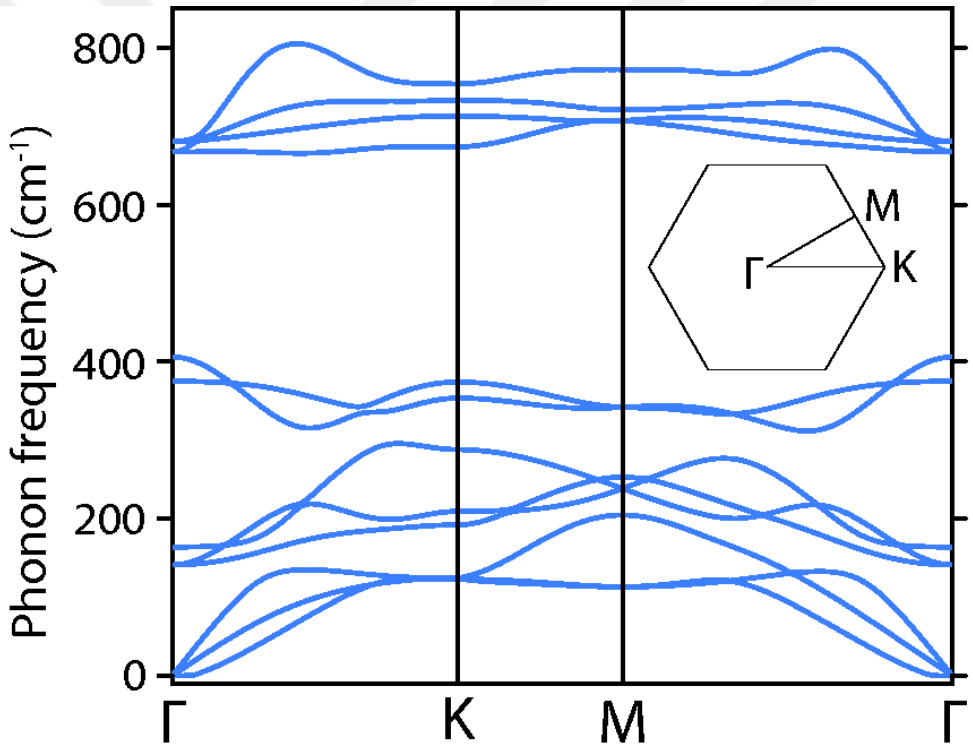

Figure 3.9: Phonon dispersion curves calculated for the bilayer of g-GaN.

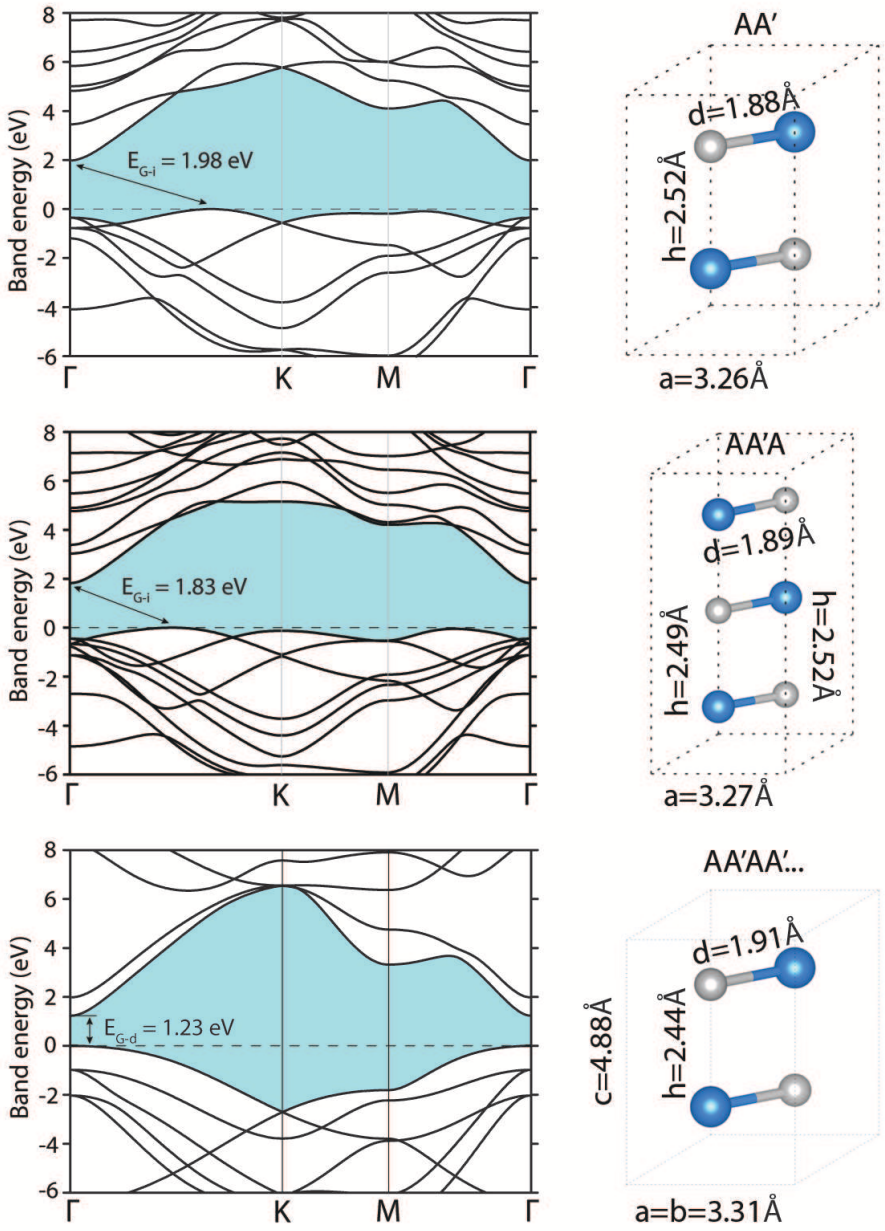

Figure 3.10: Construction of van der Waals solids by g-GaN. (a) Left: Energy band structure of bilayer b-GaN calculated using PBE with AA′ stacking. Right: Optimized atomic configuration. (b) Same as (a) for trilayer t-GaN with AA′A. (c) Same as (a) for 3D periodic layered structure p-GaN with AA′AA′... stacking. The primitive unit cell is delineated by dashed lines. Zero of energy is set to the top of the valence bands. Fundamental band gaps are shown by arrows.

3.2.5 GaN Bilayer and Multilayer Structures

Previous studies have shown that the physical properties of bilayer and multilayers of SL honeycomb structures vary slowly.[102, 103] Like SL structures, bilayer and multilayers correspond to local minima on BO surface. Growth of multilayers as well as the 3D periodic structure allow us to construct artificial materials with novel properties like van der Waals solids.[104] We explored this aspect of g-GaN and revealed their properties. Of course, we started by determining the most energetic stacking sequence, since there are a few stacking configurations. Here are the stacking sequences and (their optimized cohesive energies per Ga-N pair) for bilayer GaN i.e. b-GaN: AA$'$ (i.e. hexagons on top of each other with Ga atom being above N) [E_C=8.57 eV]; AA (Ga on Ga) [E_C=8.29 eV]; AB(GaN) (Bernal type, Ga above N) [E_C=8.49 eV]; AB(NN) which is equivalent to AB(GaGa) [E_C=8.40 eV]. Accordingly, AA$'$ sequence is found energetically favorable. The total interlayer interaction being only 280 meV, 120 meV of it is chemical interaction and remaining 160 meV has vdW character. A similar analysis has been performed for several types of stacking sequences of trilayer GaN (t-GaN) and it was found that the sequence, which is energetically most favorable is AA$'$A, with cohesive energy E_C=8.69 eV per Ga-N pair. Here the cohesive energy is larger than that of g-GaN and b-GaN, due to the increasing interlayer interaction. Note that in the cohesive energy calculation of wz- and zb-GaN, the vdW interaction is not taken into account within 3D bulk structures. Therefore, the bulk cohesive energies are slightly underestimated relative to those of the multilayer structures. The average interlayer interaction energy is 200 meV. The cohesive energies calculated for b- and t-GaN are in agreement with those of Xu *etal.*[97] The extension of b- and t-GaN is the formation of multilayer m-GaN or 3D layered p-GaN, which is periodic in the direction perpendicular to the atomic planes. We carried out calculations for the structure optimization of p-GaN. We found the stacking sequence, AA$'$AA$'$... energetically most favorable with E_C=8.94 eV per Ga-N pair.

Having determined the most energetic stacking sequence, we next tested the stability of b-GaN. Normally, if the interlayer distance is larger than the Ga-N

bond distance and the interaction among them is weak, the stability is strengthened in b-GaN. The calculation of the phonon frequencies presented in Fig. 3.9 demonstrate the stability of b-GaN and hence confirmed this conjecture.

Finally, the calculated electronic structure of b-, t-, and p-GaN are presented in Fig. 3.10, together with their optimized structures with structural parameters, such as interlayer spacing h, lattice constants a=b (c). The indirect band gap of g-GaN decreases to 1.98 eV in b-GaN and to 1.83 eV in t-GaN. Interlayer spacing h also shows this trend where it decreases with number of layers increasing, since the total interlayer interaction also increases. However, bond lengths and lattice constants display the opposite trend.

In p-GaN, the total interlayer interaction is maximized. An important outcome of this study is that, as the number of layers increases, the fundamental band gap of g-GaN decreases from 2.26 eV to 1.98 eV in b-GaN and to 1.83 eV in t-GaN. These three band gaps are indirect. However, in p-GaN, the fundamental band gap decreases to 1.23 eV and changes from indirect to direct, like in 3D wz- and zb-GaN. The crossover from indirect to direct is expected to occur in multilayer structures having less than 10 layers. It is important to note that 3D p-GaN has a direct band gap like 3D wz- and zb-GaN, nonetheless the band gap of this predicted structure is smaller by ~ 0.5 eV.

Chapter 4

Conclusions

In conclusion, in this paper we present an extensive comparative study of the 3D bulk GaN crystals and 2D graphene like single-layer honeycomb g-GaN, as well as its multilayer van der Waals solids carried out using first-principles DFT methods. While DFT provides predictions on the atomic structure, lattice constants, cohesive energy and elastic properties of 3D wz-GaN and zb-GaN crystals, it underestimates the experimentally determined fundamental band gaps by 1.5-2 eV. Here we placed an emphasis on the energetics and electronic structures, by applying state-of-the-art methods in order to improve their band gaps. For g-GaN, we performed high temperature ab-initio MD simulations showing that the stability deduced by ab-initio phonon calculations does not correspond to a shallow minimum, but the structure resists to thermal excitations by remaining stable at high temperatures. We also found that by going from 3D to 2D g-GaN, the band gap increases and is converted from direct to indirect. Additionally, state distribution in the conduction band exhibits significant changes relative to 3D wz-GaN and zb-GaN crystals. This situation is reflected to the absorption spectrum of 2D g-GaN, which is blueshifted and displays dramatic differences at higher photon energies. Finally, we found that the interaction between g-GaN and specific metallic and semiconducting substrates is weak and allows the physical properties predicted for the freestanding g-GaN to be preserved, once g-GaN is grown on such substrates. In particular, blue phosphorene is nearly lattice

matched to g-GaN, which can set weak chemical and van der Waals interactions. Accordingly, layered blue phosphorus can serve as an excellent substrate to grow single-layer or multilayer g-GaN. We hope that the present work will be insightful for growing g-GaN.

Bibliography

[1] H. Şahin, S. Cahangirov, M. Topsakal, E. Bekaroglu, E. Akturk, R. T. Senger, and S. Ciraci, "Monolayer honeycomb structures of group-iv elements and iii-v binary compounds: First-principles calculations," *Phys. Rev. B*, vol. 80, p. 155453, Oct 2009.

[2] P. Avouris, "Graphene: Electronic and photonic properties and devices," *Nano Letters*, vol. 10, no. 11, pp. 4285–4294, 2010. PMID: 20879723.

[3] F. Xia, H. Wang, D. Xiao, M. Dubey, and A. Ramasubramaniam, "Two-dimensional material nanophotonics," *Nat Photon*, vol. 8, pp. 899–907, Dec 2014. Review.

[4] M. Cambridge Electronics, "Making the new silicon," 2015.

[5] E. Sanville, S. D. Kenny, R. Smith, and G. Henkelman, "Improved grid-based algorithm for bader charge allocation," *Journal of Computational Chemistry*, vol. 28, no. 5, pp. 899–908, 2007.

[6] R. E. Peierls, "Quelques proprietes typiques des corpses solides," *Ann. I. H. Poincare*, vol. 5, pp. 177–222, 1935.

[7] L. D. Landau, "Zur Theorie der phasenumwandlungen II," *Phys. Z. Sowjetunion*, vol. 11, pp. 26–35, 1937.

[8] L. Landau and E. Lifshitz, *Statistical Physics*. No. v. 5, Elsevier Science, 2013.

[9] K. S. Novoselov, A. K. Geim, S. V. Morozov, D. Jiang, Y. Zhang, S. V. Dubonos, I. V. Grigorieva, and A. A. Firsov, "Electric field effect in atomically thin carbon films," *Science*, vol. 306, no. 5696, pp. 666–669, 2004.

[10] C. Lee, X. Wei, J. W. Kysar, and J. Hone, "Measurement of the elastic properties and intrinsic strength of monolayer graphene," *Science*, vol. 321, no. 5887, pp. 385–388, 2008.

[11] J.-H. Chen, C. Jang, S. Xiao, M. Ishigami, and M. S. Fuhrer, "Intrinsic and extrinsic performance limits of graphene devices on sio2," *Nat Nano*, vol. 3, pp. 206–209, Apr 2008.

[12] A. A. Balandin, S. Ghosh, W. Bao, I. Calizo, D. Teweldebrhan, F. Miao, and C. N. Lau, "Superior thermal conductivity of single-layer graphene," *Nano Letters*, vol. 8, no. 3, pp. 902–907, 2008. PMID: 18284217.

[13] K. Bolotin, K. Sikes, Z. Jiang, M. Klima, G. Fudenberg, J. Hone, P. Kim, and H. Stormer, "Ultrahigh electron mobility in suspended graphene," *Solid State Communications*, vol. 146, no. 910, pp. 351 – 355, 2008.

[14] Y. Zhu, S. Murali, M. D. Stoller, K. J. Ganesh, W. Cai, P. J. Ferreira, A. Pirkle, R. M. Wallace, K. A. Cychosz, M. Thommes, D. Su, E. A. Stach, and R. S. Ruoff, "Carbon-based supercapacitors produced by activation of graphene," *Science*, vol. 332, no. 6037, pp. 1537–1541, 2011.

[15] K. S. Kim, Y. Zhao, H. Jang, S. Y. Lee, J. M. Kim, K. S. Kim, J.-H. Ahn, P. Kim, J.-Y. Choi, and B. H. Hong, "Large-scale pattern growth of graphene films for stretchable transparent electrodes," *Nature*, vol. 457, pp. 706–710, Feb 2009.

[16] M. Liu, X. Yin, E. Ulin-Avila, B. Geng, T. Zentgraf, L. Ju, F. Wang, and X. Zhang, "A graphene-based broadband optical modulator," *Nature*, vol. 474, pp. 64–67, Jun 2011.

[17] O. Balci, E. O. Polat, N. Kakenov, and C. Kocabas, "Graphene-enabled electrically switchable radar-absorbing surfaces," *Nature Communications*, vol. 6, p. 6628, 2015.

[18] S. Cahangirov, M. Topsakal, E. Aktürk, H. Şahin, and S. Ciraci, "Two- and one-dimensional honeycomb structures of silicon and germanium," *Phys. Rev. Lett.*, vol. 102, p. 236804, Jun 2009.

[19] S. Cahangirov, M. Topsakal, and S. Ciraci, "Armchair nanoribbons of silicon and germanium honeycomb structures," *Phys. Rev. B*, vol. 81, p. 195120, May 2010.

[20] E. Durgun, S. Tongay, and S. Ciraci, "Silicon and iii-v compound nanotubes: Structural and electronic properties," *Phys. Rev. B*, vol. 72, p. 075420, Aug 2005.

[21] P. Vogt, P. De Padova, C. Quaresima, J. Avila, E. Frantzeskakis, M. C. Asensio, A. Resta, B. Ealet, and G. Le Lay, "Silicene: Compelling experimental evidence for graphenelike two-dimensional silicon," *Phys. Rev. Lett.*, vol. 108, p. 155501, Apr 2012.

[22] P. De Padova, C. Quaresima, C. Ottaviani, P. M. Sheverdyaeva, P. Moras, C. Carbone, D. Topwal, B. Olivieri, A. Kara, H. Oughaddou, B. Aufray, and G. Le Lay, "Evidence of graphene-like electronic signature in silicene nanoribbons," *Applied Physics Letters*, vol. 96, no. 26, 2010.

[23] M. E. Dávila and G. Le Lay, "Few layer epitaxial germanene: a novel two-dimensional dirac material," *Scientific Reports*, vol. 6, pp. 20714 EP –, Feb 2016. Article.

[24] L. Tao, E. Cinquanta, D. Chiappe, C. Grazianetti, M. Fanciulli, M. Dubey, A. Molle, and D. Akinwande, "Silicene field-effect transistors operating at room temperature," *Nat Nano*, vol. 10, pp. 227–231, Mar 2015. Letter.

[25] F.-f. Zhu, W.-j. Chen, Y. Xu, C.-l. Gao, D.-d. Guan, C.-h. Liu, D. Qian, S.-C. Zhang, and J.-f. Jia, "Epitaxial growth of two-dimensional stanene," *Nat Mater*, vol. 14, pp. 1020–1025, Oct 2015. Article.

[26] Y. Xu, B. Yan, H.-J. Zhang, J. Wang, G. Xu, P. Tang, W. Duan, and S.-C. Zhang, "Large-gap quantum spin hall insulators in tin films," *Phys. Rev. Lett.*, vol. 111, p. 136804, Sep 2013.

[27] C. Ataca, H. Sahin, and S. Ciraci, "Stable, single-layer mx2 transition-metal oxides and dichalcogenides in a honeycomb-like structure," *The Journal of Physical Chemistry C*, vol. 116, no. 16, pp. 8983–8999, 2012.

[28] J. Wilson and A. Yoffe, "The transition metal dichalcogenides discussion and interpretation of the observed optical, electrical and structural properties," *Advances in Physics*, vol. 18, no. 73, pp. 193–335, 1969.

[29] E. A. Marseglia, "Transition metal dichalcogenides and their intercalates," *International Reviews in Physical Chemistry*, vol. 3, no. 2, pp. 177–216, 1983.

[30] A. Ayari, E. Cobas, O. Ogundadegbe, and M. S. Fuhrer, "Realization and electrical characterization of ultrathin crystals of layered transition-metal dichalcogenides," *Journal of Applied Physics*, vol. 101, no. 1, 2007.

[31] H. Liu, A. T. Neal, Z. Zhu, Z. Luo, X. Xu, D. Tomanek, and P. D. Ye, "Phosphorene: An unexplored 2D semiconductor with a high hole mobility," *ACS Nano*, vol. 8, no. 4, pp. 4033–4041, 2014.

[32] L. Li, Y. Yu, G. J. Ye, Q. Ge, X. Ou, H. Wu, D. Feng, X. H. Chen, and Y. Zhang, "Black phosphorus field-effect transistors.," *Nature nanotechnology*, vol. 9, no. 5, pp. 372–7, 2014.

[33] V. O. Özçelik, O. U. Aktürk, E. Durgun, and S. Ciraci, "Prediction of a two-dimensional crystalline structure of nitrogen atoms," *Phys. Rev. B*, vol. 92, p. 125420, Sep 2015.

[34] O. U. Aktürk, V. O. Özçelik, and S. Ciraci, "Single-layer crystalline phases of antimony: Antimonenes," *Phys. Rev. B*, vol. 91, p. 235446, Jun 2015.

[35] E. Bekaroglu, M. Topsakal, S. Cahangirov, and S. Ciraci, "First-principles study of defects and adatoms in silicon carbide honeycomb structures," *Phys. Rev. B*, vol. 81, p. 075433, Feb 2010.

[36] M. Topsakal, S. Cahangirov, E. Bekaroglu, and S. Ciraci, "First-principles study of zinc oxide honeycomb structures," *Phys. Rev. B*, vol. 80, p. 235119, Dec 2009.

[37] D. Paciele, J. C. Meyer, c. O. Girit, and A. Zettl, "The two-dimensional phase of boron nitride: Few-atomic-layer sheets and suspended membranes," *Applied Physics Letters*, vol. 92, no. 13, pp. 24–27, 2008.

[38] Y. Kubota, K. Watanabe, O. Tsuda, and T. Taniguchi, "Deep ultraviolet light-emitting hexagonal boron nitride synthesized at atmospheric pressure," *Science*, vol. 317, no. 5840, pp. 932–934, 2007.

[39] K. Watanabe, T. Taniguchi, and H. Kanda, "Direct-bandgap properties and evidence for ultraviolet lasing of hexagonal boron nitride single crystal," *Nat Mater*, vol. 3, pp. 404–409, Jun 2004.

[40] D. R., Y. F., MericI., LeeC., WangL., SorgenfreiS., WatanabeK., TaniguchiT., KimP., S. L., and HoneJ., "Boron nitride substrates for high-quality graphene electronics," *Nat Nano*, vol. 5, pp. 722–726, Oct 2010.

[41] J. Xue, J. Sanchez-Yamagishi, D. Bulmash, P. Jacquod, A. Deshpande, K. Watanabe, T. Taniguchi, P. Jarillo-Herrero, and B. J. LeRoy, "Scanning tunnelling microscopy and spectroscopy of ultra-flat graphene on hexagonal boron nitride," *Nat Mater*, vol. 10, pp. 282–285, Apr 2011.

[42] P. Tsipas, S. Kassavetis, D. Tsoutsou, E. Xenogiannopoulou, E. Golias, S. A. Giamini, C. Grazianetti, D. Chiappe, A. Molle, M. Fanciulli, and A. Dimoulas, "Evidence for graphite-like hexagonal aln nanosheets epitaxially grown on single crystal ag(111)," *Applied Physics Letters*, vol. 103, no. 25, 2013.

[43] D. Kecik, C. Bacaksiz, R. T. Senger, and E. Durgun, "Layer- and strain-dependent optoelectronic properties of hexagonal aln," *Phys. Rev. B*, vol. 92, p. 165408, Oct 2015.

[44] S. Nakamura, "Nobel lecture: Background story of the invention of efficient blue ingan light emitting diodes*," *Rev. Mod. Phys.*, vol. 87, pp. 1139–1151, Oct 2015.

[45] H. Morkoç, *Handbook of Nitride Semiconductors and Devices, GaN-based Optical and Electronic Devices*. Handbook of Nitride Semiconductors and Devices, Wiley, 2009.

[46] M. Born and R. Oppenheimer, "Zur quantentheorie der molekeln," *Annalen der Physik*, vol. 389, no. 20, pp. 457–484, 1927.

[47] D. R. Hartree, "The wave mechanics of an atom with a non-coulomb central field. part i. theory and methods," *Mathematical Proceedings of the Cambridge Philosophical Society*, vol. 24, pp. 89–110, 1 1928.

[48] P. Hohenberg and W. Kohn, "Inhomogeneous electron gas," *Phys. Rev.*, vol. 136, pp. B864–B871, Nov 1964.

[49] W. Kohn and L. J. Sham, "Self-consistent equations including exchange and correlation effects," *Phys. Rev.*, vol. 140, pp. A1133–A1138, Nov 1965.

[50] A. D. Becke, "A new mixing of hartreefock and local density-functional theories," *The Journal of Chemical Physics*, vol. 98, no. 2, 1993.

[51] J. Heyd, G. E. Scuseria, and M. Ernzerhof, "Hybrid functionals based on a screened coulomb potential," *The Journal of Chemical Physics*, vol. 118, no. 18, 2003.

[52] J. Klime and A. Michaelides, "Perspective: Advances and challenges in treating van der waals dispersion forces in density functional theory," *The Journal of Chemical Physics*, vol. 137, no. 12, 2012.

[53] T. Bucko, J. Hafner, S. Lebgue, and J. G. ngyn, "Improved description of the structure of molecular and layered crystals: Ab initio dft calculations with van der waals corrections," *The Journal of Physical Chemistry A*, vol. 114, no. 43, pp. 11814–11824, 2010. PMID: 20923175.

[54] H. J. Monkhorst and J. D. Pack, "Special points for brillouin-zone integrations," *Phys. Rev. B*, vol. 13, pp. 5188–5192, Jun 1976.

[55] M. Gajdoš, K. Hummer, G. Kresse, J. Furthmüller, and F. Bechstedt, "Linear optical properties in the projector-augmented wave methodology," *Phys. Rev. B*, vol. 73, p. 045112, Jan 2006.

[56] G. Kresse and J. Hafner, "*Ab initio* molecular dynamics for liquid metals," *Phys. Rev. B*, vol. 47, pp. 558–561, Jan 1993.

[57] G. Kresse and J. Hafner, "*Ab initio* molecular-dynamics simulation of the liquid-metal˘amorphous-semiconductor transition in germanium," *Phys. Rev. B*, vol. 49, pp. 14251–14269, May 1994.

[58] G. Kresse and J. Furthmller, "Efficiency of ab-initio total energy calculations for metals and semiconductors using a plane-wave basis set," *Computational Materials Science*, vol. 6, no. 1, pp. 15 – 50, 1996.

[59] G. Kresse and J. Furthmüller, "Efficient iterative schemes for *ab initio* total-energy calculations using a plane-wave basis set," *Phys. Rev. B*, vol. 54, pp. 11169–11186, Oct 1996.

[60] J. P. Perdew, K. Burke, and M. Ernzerhof, "Generalized gradient approximation made simple," *Phys. Rev. Lett.*, vol. 77, pp. 3865–3868, Oct 1996.

[61] J. P. Perdew, K. Burke, and M. Ernzerhof, "Generalized gradient approximation made simple," *Phys. Rev. Lett.*, vol. 78, pp. 1396–1396, Feb 1997.

[62] S. Grimme, "Semiempirical gga-type density functional constructed with a long-range dispersion correction," *Journal of Computational Chemistry*, vol. 27, no. 15, pp. 1787–1799, 2006.

[63] D. Alf, "Phon: A program to calculate phonons using the small displacement method," *Computer Physics Communications*, vol. 180, no. 12, pp. 2622 – 2633, 2009. 40 {YEARS} {OF} CPC: A celebratory issue focused on quality software for high performance, grid and novel computing architectures.

[64] S. Baroni, S. de Gironcoli, A. Dal Corso, and P. Giannozzi, "Phonons and related crystal properties from density-functional perturbation theory," *Rev. Mod. Phys.*, vol. 73, pp. 515–562, Jul 2001.

[65] S. Nos, "A unified formulation of the constant temperature molecular dynamics methods," *The Journal of Chemical Physics*, vol. 81, no. 1, 1984.

[66] J. Paier, M. Marsman, K. Hummer, G. Kresse, I. C. Gerber, and J. G. ngyn, "Screened hybrid density functionals applied to solids," *The Journal of Chemical Physics*, vol. 124, no. 15, 2006.

[67] J. Heyd and G. E. Scuseria, "Assessment and validation of a screened coulomb hybrid density functional," *The Journal of Chemical Physics*, vol. 120, no. 16, 2004.

[68] L. Hedin, "New method for calculating the one-particle green's function with application to the electron-gas problem," *Phys. Rev.*, vol. 139, pp. A796–A823, Aug 1965.

[69] M. S. Hybertsen and S. G. Louie, "Electron correlation in semiconductors and insulators: Band gaps and quasiparticle energies," *Phys. Rev. B*, vol. 34, pp. 5390–5413, Oct 1986.

[70] M. Shishkin and G. Kresse, "Implementation and performance of the frequency-dependent *gw* method within the paw framework," *Phys. Rev. B*, vol. 74, p. 035101, Jul 2006.

[71] Q. Yan, P. Rinke, A. Janotti, M. Scheffler, and C. G. Van de Walle, "Effects of strain on the band structure of group-iii nitrides," *Phys. Rev. B*, vol. 90, p. 125118, Sep 2014.

[72] K. Karch, J.-M. Wagner, and F. Bechstedt, "*Ab initio* study of structural, dielectric, and dynamical properties of gan," *Phys. Rev. B*, vol. 57, pp. 7043–7049, Mar 1998.

[73] F. Bernardini, V. Fiorentini, and D. Vanderbilt, "Spontaneous polarization and piezoelectric constants of iii-v nitrides," *Phys. Rev. B*, vol. 56, pp. R10024–R10027, Oct 1997.

[74] F. Bechstedt, U. Grossner, and J. Furthmüller, "Dynamics and polarization of group-iii nitride lattices: A first-principles study," *Phys. Rev. B*, vol. 62, pp. 8003–8011, Sep 2000.

[75] M. Magnuson, M. Mattesini, C. Höglund, J. Birch, and L. Hultman, "Electronic structure of gan and ga investigated by soft x-ray spectroscopy and first-principles methods," *Phys. Rev. B*, vol. 81, p. 085125, Feb 2010.

[76] M. A. Caro, S. Schulz, and E. P. O'Reilly, "Theory of local electric polarization and its relation to internal strain: Impact on polarization potential and

electronic properties of group-iii nitrides," *Phys. Rev. B*, vol. 88, p. 214103, Dec 2013.

[77] Z. Dridi, B. Bouhafs, and P. Ruterana, "First-principles investigation of lattice constants and bowing parameters in wurtzite al x ga 1- x n, in x ga 1- x n and in x al 1- x n alloys," *Semiconductor Science and Technology*, vol. 18, no. 9, p. 850, 2003.

[78] J. Heyd, J. E. Peralta, G. E. Scuseria, and R. L. Martin, "Energy band gaps and lattice parameters evaluated with the heyd-scuseria-ernzerhof screened hybrid functional," *The Journal of Chemical Physics*, vol. 123, no. 17, 2005.

[79] P. Rinke, M. Winkelnkemper, A. Qteish, D. Bimberg, J. Neugebauer, and M. Scheffler, "Consistent set of band parameters for the group-iii nitrides aln, gan, and inn," *Phys. Rev. B*, vol. 77, p. 075202, Feb 2008.

[80] H. Schulz and K. Thiemann, "Crystal structure refinement of aln and gan," *Solid State Communications*, vol. 23, no. 11, pp. 815 – 819, 1977.

[81] I. Vurgaftman and J. R. Meyer, "Band parameters for nitrogen-containing semiconductors," *Journal of Applied Physics*, vol. 94, no. 6, 2003.

[82] H. Xia, Q. Xia, and A. L. Ruoff, "High-pressure structure of gallium nitride: Wurtzite-to-rocksalt phase transition," *Phys. Rev. B*, vol. 47, pp. 12925–12928, May 1993.

[83] M. Ueno, M. Yoshida, A. Onodera, O. Shimomura, and K. Takemura, "Stability of the wurtzite-type structure under high pressure: Gan and inn," *Phys. Rev. B*, vol. 49, pp. 14–21, Jan 1994.

[84] P. Perlin, C. Jauberthie-Carillon, J. P. Itie, A. San Miguel, I. Grzegory, and A. Polian, "Raman scattering and x-ray-absorption spectroscopy in gallium nitride under high pressure," *Phys. Rev. B*, vol. 45, pp. 83–89, Jan 1992.

[85] C. Bungaro, K. Rapcewicz, and J. Bernholc, "*Ab initio* phonon dispersions of wurtzite aln, gan, and inn," *Phys. Rev. B*, vol. 61, pp. 6720–6725, Mar 2000.

[86] A. F. Wright and J. S. Nelson, "Explicit treatment of the gallium 3 d electrons in gan using the plane-wave pseudopotential method," *Phys. Rev. B*, vol. 50, pp. 2159–2165, Jul 1994.

[87] A. Polian, M. Grimsditch, and I. Grzegory, "Elastic constants of gallium nitride," *Journal of Applied Physics*, vol. 79, no. 6, 1996.

[88] Y. Du, B. Chang, X. Fu, X. Wang, and M. Wang, "Electronic structure and optical properties of zinc-blende gan," *Optik - International Journal for Light and Electron Optics*, vol. 123, no. 24, pp. 2208 – 2212, 2012.

[89] X.-Z. Li, R. Gmez-Abal, H. Jiang, C. Ambrosch-Draxl, and M. Scheffler, "Impact of widely used approximations to the g 0 w 0 method: an all-electron perspective," *New Journal of Physics*, vol. 14, no. 2, p. 023006, 2012.

[90] M. Rohlfing, P. Krüger, and J. Pollmann, "Role of semicore d electrons in quasiparticle band-structure calculations," *Phys. Rev. B*, vol. 57, pp. 6485–6492, Mar 1998.

[91] P. Rinke, A. Qteish, J. Neugebauer, C. Freysoldt, and M. Scheffler, "Combining gw calculations with exact-exchange density-functional theory: an analysis of valence-band photoemission for compound semiconductors," *New Journal of Physics*, vol. 7, no. 1, p. 126, 2005.

[92] G. Ramírez-Flores, H. Navarro-Contreras, A. Lastras-Martínez, R. C. Powell, and J. E. Greene, "Temperature-dependent optical band gap of the metastable zinc-blende structure β-gan," *Phys. Rev. B*, vol. 50, pp. 8433–8438, Sep 1994.

[93] M. E. Sherwin and T. J. Drummond, "Predicted elastic constants and critical layer thicknesses for cubic phase aln, gan, and inn on -sic," *Journal of Applied Physics*, vol. 69, no. 12, 1991.

[94] C. R. Company, "Crc handbook of chemistry and physics," 1978. A ready-reference book of chemical and physical data.

[95] W. A. Harrison and S. Ciraci, "Bond-orbital model. ii," *Phys. Rev. B*, vol. 10, pp. 1516–1527, Aug 1974.

[96] Q. Peng, C. Liang, W. Ji, and S. De, "Mechanical properties of g-gan: a first principles study," *Applied Physics A*, vol. 113, no. 2, pp. 483–490, 2013.

[97] D. Xu, H. He, R. Pandey, and S. P. Karna, "Stacking and electric field effects in atomically thin layers of gan," *Journal of Physics: Condensed Matter*, vol. 25, no. 34, p. 345302, 2013.

[98] Q. Chen, H. Hu, X. Chen, and J. Wang, "Tailoring band gap in gan sheet by chemical modification and electric field: Ab initio calculations," *Applied Physics Letters*, vol. 98, no. 5, 2011.

[99] C. Attaccalite, A. Nguer, E. Cannuccia, and M. Gruning, "Strong second harmonic generation in sic, zno, gan two-dimensional hexagonal crystals from first-principles many-body calculations," *Phys. Chem. Chem. Phys.*, vol. 17, pp. 9533–9540, 2015.

[100] H. L. Zhuang, A. K. Singh, and R. G. Hennig, "Computational discovery of single-layer iii-v materials," *Phys. Rev. B*, vol. 87, p. 165415, Apr 2013.

[101] C. Kittel, *Introduction to Solid State Physics*. John Wiley & Sons, Inc., 2010.

[102] S. Cahangirov, V. O. Özçelik, L. Xian, J. Avila, S. Cho, M. C. Asensio, S. Ciraci, and A. Rubio, "Atomic structure of the $\sqrt{3} \times \sqrt{3}$ phase of silicene on ag(111)," *Phys. Rev. B*, vol. 90, p. 035448, Jul 2014.

[103] S. Cahangirov, V. O. Özçelik, A. Rubio, and S. Ciraci, "Silicite: The layered allotrope of silicon," *Phys. Rev. B*, vol. 90, p. 085426, Aug 2014.

[104] A. K. Geim and I. V. Grigorieva, "Van der waals heterostructures," *Nature*, vol. 499, pp. 419–425, Jul 2013.